공학석사 학위논문

A Coupled Phase Diagram Experiment and the Thermodynamic Modeling of the $ZnO-SnO_2-SiO_2$ System

$ZnO-SnO_2-SiO_2$ 3원계 시스템의 상태도 실험과
열역학 모델링

2020 년 8 월

서울대학교 대학원
재료공학부
이 재 성

A Coupled Phase Diagram Experiment and the Thermodynamic Modeling of the $ZnO-SnO_2-SiO_2$ System

지도 교수 정 인 호

이 논문을 공학석사 학위논문으로 제출함

2020 년 08 월

서울대학교 대학원

재료공학과

이 재 성

이재성의 공학석사 학위논문을 인준함

2020 년 08 월

위 원 장 유 상 임 (인)

부위원장 정 인 호 (인)

위 원 홍 성 현 (인)

Abstract

The development of an accurate thermodynamic database to calculate the thermodynamic properties and phase equilibria in complex systems plays an important role in the development of many ceramic and metallurgical processes. Thermodynamic database is developed by the comprehensive critical evaluation and optimization of all the thermodynamic property and phase diagram data.

As part of a large thermodynamic database development for glassmaking and metallurgical applications, the entire ZnO-SnO_2-SiO_2 system was critically evaluated and optimized. Due to the lack of phase diagram experiment data in the ZnO-SnO_2, SnO_2-SiO_2, and the ternary ZnO-SnO_2-SiO_2 system, the phase equilibria in the binary and ternary systems were determined using the classical quenching experiments and differential thermal analysis (DTA) followed by X-ray diffraction (XRD) analysis and electron probe micro-analysis (EPMA). Sealed platinum capsules were employed for preventing the evaporation of ZnO and SnO_2 in the experiments. In the course of the optimization, the melting temperature of SnO_2 was re-evaluated. The phase diagrams of ZnO-SnO_2, SnO_2-SiO_2, and ZnO-SnO_2-SiO_2 systems were constructed for the first time. By using the construct thermodynamic database containing the Gibbs energy functions of all phases in the ternary system,

phase equilibria and the thermodynamic properties within the ternary system could be accurately calculated. All the thermodynamic calculations and optimization in the present study were carried out using the FactSage™ thermochemical software.

Keywords: ZnO-SnO_2-SiO_2, ZnO_2-SnO_2, SnO_2-SiO_2, ZnO-SiO_2, Zn_2SnO_4, Phase Diagram, Thermodynamics, CALPHAD

Table of Contents

List of Figures

List of Tables

Chapter 1. Introduction

1.1. Research Objective

Both ZnO and SnO_2 are common components in engineering glass. In addition, the thermodynamic behavior of these oxides in molten silicate is important for the pyrometallurgical recycling processes of industrial wastes. However, the accurate and reliable phase diagrams containing SnO_2 and ZnO have not been well studied. The goal of this study is to develop a self-consistent thermodynamic database with high accuracy and predictability of the ZnO-SnO_2-SiO_2 system. Calculation of PHAse Diagram (CALPHAD) methodology was used to develop the present thermodynamic database. In the CALPHAD database development, all available experimental phase diagram and thermodynamic property data are critically evaluated and optimized to find the one set of self-consistent Gibbs energy functions of all phases in the system. If necessary, new phase diagram and thermodynamic property measurement can be performed to assist the database development. Based on the new experimental data and available literature data, the optimization of the ternary ZnO-SnO_2-SiO_2 system was completed. In order to construct the accurate database of the ZnO-SnO_2-SiO_2 ternary system, the phase diagram experiments for ZnO-SnO_2, SnO_2-SiO_2, and ternary ZnO-SnO_2-SiO_2 systems were carried out.

1.2. Organization

The present thesis is composed of the following chapters:

Chapter 2 explains CALPHAD type thermodynamic optimization and all the thermodynamic models to describe the solid and liquid phases present in the ZnO-SnO_2-SiO_2 system.

Chapter 3 presents the key phase diagram experiments and optimization results of the binary ZnO-SnO_2 and SnO_2-SiO_2 systems. Materials preparation, experimental procedures, and characterization techniques used to define the phase diagram of ZnO-SnO_2 and SnO_2-SiO_2 systems are presented. Details of the thermodynamic optimization process of the two binary systems are also explained. ZnO-SiO_2 system was previously modeled by Konar in 2018 (unpublished work), and the optimization for the system was taken with little modifications.

Chapter 4 contains the key phase diagram experiment and the optimization results for the ternary ZnO-SnO_2-SiO_2 system. Materials preparation, experimental procedures, and characterization techniques are also presented.

Conclusion summarizes all the work done in the present study and lists up

suggestions for future work.

Chapter 2. Thermodynamic Optimization and the CALculation of PHAse Diagrams (CALPHAD) Approach

2.1. Thermodynamic Optimization

The main goal of the CALPHAD thermodynamic optimization is to obtain a set of model equations of Gibbs energies for all phases as a function of temperature and composition. Measurement of thermodynamic properties and phase diagram helps to deduce the Gibbs energies of phases. During optimization, discrepancies between inconsistent data should be resolved, and interpolations and extrapolations must be made abiding to the principles of thermodynamics. Once a system of interest is chosen, a thermodynamic database needs to be built from a low-order system (unary and binary) to high-order system (ternary, quaternary, …), which eventually can be applied to complex industrial processes.

Basic procedures of thermodynamic optimization are as follows:

1. The system of industrial interest is defined.

2. Related literature data are collected. These data include:

a) Thermodynamic data: Thermodynamic data including chemical activities, phase equilibria between solid, liquid, and gas, calorimetric data (enthalpy of formation, mixing, and heat capacity), vapor pressure (Knudsen cell), chemical potential (electromotive force measurements), etc. are collected. Data available in practical high-order system may be useful to estimate the thermodynamic property of the low-order sub system by interpolation or extrapolation.

b) Crystal structure data: These data can be used to predict the thermodynamic properties of solid solutions. Also, these data are helpful to identify what solutions should be considered in the given system.

c) Reliability of the available data must also be assessed at this point. Experiments aimed to produce data for the same purpose might be different with each other over acceptable experimental error limits. Moreover, a compilation of thermodynamic property data and phase equilibrium experiments may yield contradicting results. Thus, all experimental data need to be organized and assessed accordingly to their experimental techniques, experimental conditions, and analytical methods. Often, literatures also may not provide enough information to accurately determine their experimental

techniques, conditions, and analytical methods. These sources of error can also be judged during the critical evaluation and optimization.

3. If there are no available data or if the data available are unreliable, thermodynamic property measurements and/or coupled phase diagram experiments can be conducted to assist thermodynamic optimization.

4. A suitable model to represent the Gibbs energy function of each phase should be selected. A solution model should be selected to reflect the structure of the solution phase. A good thermodynamic model can predict the thermodynamic properties and phase diagram data in the multicomponent systems from the model parameters of the low-order systems.

5. Model parameters for each phase are optimized based on the reliable experimental data. Optimization is done with the aid of FactSage^{TM} (version 7.3) thermochemical software [1]. Optimizations of model parameters continue until they can accurately back-calculate and produce all reliable experimental data within experimental error limits.

6. Various predictions and thermodynamic calculations are performed using the developed thermodynamic database. Predictions on the phase equilibria of higher order systems can be conducted for practical applications.

2.2. Thermodynamic Models

Thermodynamics models are crucial to understanding and representing the thermodynamic properties and phase equilibria of materials. Appropriate thermodynamic model is powerful because it goes beyond just to presenting thermal properties. For example, it can provide the structural information of solutions, which can be used to understand the physical and electrical properties of them. In this study, the liquid solutions were modeled using the Modified Quasichemical Model (MQM). All solid phases were accounted as stoichiometric and no solid solutions were considered. The ZnO-SiO_2 system was optimized previously by Konar (unpublished work, 2018). The thermodynamic optimization results were adopted without large modifications in this study.

2.2.1. Stoichiometric Compounds

The Gibbs energy of a stoichiometric compound can be expressed as the following:

$$g_T^o = h_T^o - Ts_T^o$$

$$h_T^o = \Delta h_{298.15}^o + \int_{298.15}^{T} c_p dT$$

$$s_T^o = s_{298.15}^o + \int_{298.15}^{T} {}^{c_p}/_{T}\ dT$$

in which g_T^o, h_T^o, and s_T^o are the standard molar Gibbs energy, enthalpy, and entropy of a stoichiometric compound, respectively, at the absolute temperature T. c_p is the heat capacity of a compound which is a function of temperature. $\Delta h_{298.15}^o$ is the standard enthalpy of formation at 298.15K, and by definition and convention, $\Delta h_{298.15}^o$ of a stable elemental species (at 1atm and 298.15K) is 0J/mol. $s_{298.15}^o$ is the standard molar entropy at 298.15K.

In this work, the Gibbs energies of pure components including liquid SnO, solid Sn_3O_4, solid and liquid SiO_2 and ZnO, and solid SnO_2 were taken from the optimized in the FactSage™ database [1]. The Gibbs energy of liquid SnO_2 was reoptimized as the melting point of the compound was redefined in this study. The methodology and the logic behind the re-optimization of the Gibbs energy of SnO_2 is outlined in the appendix.

In the SnO_2-SiO_2 system, no intermediate stoichiometric compound has been reported. In the ZnO-SnO_2 system, the Gibbs energy of one binary compound, Zn_2SnO_4, was optimized based on the experimental and thermodynamic property data [2]. The Gibbs energy of reported stoichiometric compounds in the binary systems containing SnO_2 (SnO_2-CaO, SnO_2-MgO, SnO_2-CoO)

were optimized as well and the results are presented also in the appendix.

2.2.2. Liquid Solution

For a pure component A, the molar Gibbs energy can be written as the following:

$$g_A^o = h_A^o - Ts_A^o$$

in which g_A^o, h_A^o, and s_A^o each represent standard molar Gibbs energy, enthalpy, entropy of component A. T is the absolute temperature.

When two components A and B are mixed, the properties of the solution rely on the interaction between A and B. If the interaction between A and B is ideal, the Gibbs energy of the solution can be written as:

$$G^m = (n_A g_A^o + n_B g_B^o) - T\Delta S^{config}$$

$$\Delta S^{config} = -R(n_A \ln X_A + n_B \ln X_B)$$

where G^m is the Gibbs energy of the solution, g_A^o and g_B^o are the molar Gibbs energy of the component A and B, and ΔS^{config} is the configurational

entropy obtained by mixing n_A moles of component A and n_B moles of component B. X_A and X_B represent the mol fractions of each component.

In an ideal solution, the excess interaction between A and B is zero. For a non-ideal solution, the interaction between A and B is not zero, and the non-ideal term can be quantified as the molar excess Gibbs energy of the solution (g^E). Thus, the Gibbs energy of the non-ideal solution can be written as:

$$G^m = (n_A g_A^o + n_B g_B^o) - T\Delta S^{config} + (n_A + n_B)g^E$$

$$g^E = \sum q_{AB}^{ij} X_A^i X_B^j$$

$$q_{AB}^{ij} = a + bT + cT^2 + \cdots$$

in which X_A^i and X_B^j are the mole fractions of component A and B in the solution phase. q_{AB}^{ij} is an excess interaction parameter term. The well-known regular solution only utilizes q_{AB}^{11} excess term to describe the excess Gibbs energy of the solution.

In the case that the liquid solution deviates largely from an ideal solution, configuration entropy no longer becomes close to that of an ideal solution. To

describe the Gibbs energy of liquid oxide typically deviating largely from an ideal solution, Modified Quasichemical Model (MQM) [3] has been widely used. In the MQM description of binary solution, the pair exchange reaction between the second-nearest-neighbor (SNN) cationic species of A and B in oxide melt is considered:

$$(A-A)+(B-B)=2(A-B) \qquad \Delta g_{AB}$$

in which A and B are cationic species in a solution and $(A-B)$ represents a SNN pair, with oxygen as the bridging anion. Δg_{AB}, the Gibbs energy of the pair exchange reaction represents the change in the non-configurational Gibbs energy induced by the formation of $(A-B)$ pairs.

The Gibbs energy of a solution is represented by:

$$G^m=(n_A g_A^o+n_B g_B^o)-T\Delta S^{config}+\left(\frac{n_{AB}}{2}\right)\Delta g_{AB}$$

where n_A, n_B, g_A^o, and g_B^o are the number of moles and molar Gibbs energies of the pure components A and B and n_{AB} is the number of moles of $(A-B)$ pair bonds at the equilibrium. ΔS^{config} is configurational entropy which considers the random distribution of $(A-A)$, $(B-B)$, and $(A-B)$ pair by one dimensional Ising model [4].

The configurational entropy is represented by:

$$\Delta S^{conf} = -RT(n_A \ln X_A + n_B \ln X_B) - R(n_{AA} \ln\left(\frac{X_{AA}}{Y_A^2}\right) + n_{BB} \ln\left(\frac{X_{BB}}{Y_B^2}\right) + n_{AB} \ln\left(\frac{X_{AB}}{2Y_A Y_B}\right))$$

$$X_A = \frac{n_A}{n_A + n_B} = 1 - X_B$$

$$X_{ij} = \frac{n_{ij}}{n_{AA} + n_{AB} + n_{BB}}$$

$$Y_A = \frac{n_A Z_A}{n_A Z_A + n_B Z_B}$$

in which X_A and X_B are site fractions, X_{AA}, X_{BB}, X_{AB} are pair fractions, Y_A and Y_B are coordination-equivalent fractions, and Z_A and Z_B are the coordination number of A and B.

Δg_{AB} can be expanded as a function of pair fractions:

$$\Delta g_{AB} = \Delta g^{\circ}_{AB} + \sum_{i \geq 1} g^{i0}_{AB} X^i_{AA} + \sum_{i \geq 1} g^{0j}_{AB} X^j_{BB}$$

Δg°_{AB}, g^{i0}_{AB}, and g^{0j}_{AB} are model parameters that may be functions of temperature.

After all binary systems are thermodynamically optimized and defined, thermodynamic properties of ternary solution are calculated from the binary model parameters using "geometric" models elaborated by Pelton [5].

$$g_{sol} = \sum g_i^o x_i - T\Delta S^{conf} + g^E$$

in which g_{sol} is the molar Gibbs energy of a solution, and g_i^o is the molar Gibbs energy of a pure component i. ΔS^{conf} is configurational entropy, and g^E is extrapolated from binary model parameters and may also contain excess ternary Gibbs energy parameters.

Multiple "geometric" models have been developed to accurately predict the thermodynamic properties of ternary systems from the combination of three binary systems. The models are dependent on the properties of the binary systems. These are illustrated in Figure 2.1. Depending on the model, the excess Gibbs energy (g^E) at any composition "p" of a solution is calculated differently based on the Gibbs energies of binary sub-systems at points a, b, and c.

The excess Gibbs energy of a ternary solution can be written as the following:

$$g^E = \frac{X_{12}\Delta g_{12}}{2} + \frac{X_{13}\Delta g_{13}}{2} + \frac{X_{23}\Delta g_{23}}{2} + q_{123}^{ijk} X_1^i X_2^j X_3^k$$

in which Δg_{ij} represents the Gibbs energy difference for the following reaction of

$$(i - i) + (j - j) = 2(i - j) \qquad \Delta g_{ij}$$

$q_{123}^{ijk} X_1^i X_2^j X_3^k$ is a ternary term that can be used to estimate interactions in a ternary system. q_{123}^{ijk} is an empirical coefficient.

Ideally, ternary terms should be close to zero or as small as possible. Large value of the ternary term may cast doubts on the predictability and reliability of the model.

The Kohler/Toop and Muggianu/Toop models are “asymmetric” models Muggianu and Kohler models are “symmetric” models. An asymmetric model is used when two components are chemically similar, and one component is chemically different. Mixing enthalpies of the binary system, charges of each components, etc. can be some of the deciding factors. If the components are chemically similar, symmetric models are used. The different

interpolation techniques can give radically different results when g^E is large and Δg_{ij} is largely dependent on compositions. Improper choices of the ternary interpolation techniques can lead to a difficulty in the development of a large database.

The MQM description of the excess Gibbs energy of a ternary solution was given by Chartrand and Pelton [6]. If a symmetric Kohler-type approximation is chosen for a 1-2 subsystem, Δg_{12} in the g^E equation is given as the following:

$$\Delta g_{12} = \Delta g_{12}^0 + \sum_{l\leq(i+j)} g_{12}^{ij} \left(\frac{X_{11}}{X_{11}+X_{12}+X_{22}}\right)^i \left(\frac{X_{22}}{X_{11}+X_{12}+X_{22}}\right)^j$$

If an asymmetric Toop-type approximation is chosen, Δg_{12} can be expressed as:

$$\Delta g_{12} = \Delta g_{12}^0 + \sum_{l\leq(i+j)} g_{12}^{ij} X_{11}^i (X_{22} + X_{23} + X_{33})^j$$

where Δg_{12}^0 and g_{12}^{ij} are the model parameters of the binary 1-2 system.

The FactSage™ thermochemical software [1] allows a user to choose any interpolation technique for each ternary system. The interpolation technique

used in the present ZnO-SnO_2-SiO_2 solution will be discussed later in Chapter 4.

2.2.3. Metallic and Gas Phases

The gas phases of all species (O, O_2, O_3, Sn, SnO, SnO_2, Sn_2O_2, Sn_3O_3, Sn_4O_4, Si, Si_2, Si_3, SiO, SiO_2, Zn) were taken from the FACT pure substance database [1]. In the appendix, the Sn-O phase diagram is re-optimized. To calculate the metallic Sn saturation condition in the Sn-O system, the solid Sn and liquid Sn solution from FTmisc database was considered (SnLQ) [7].

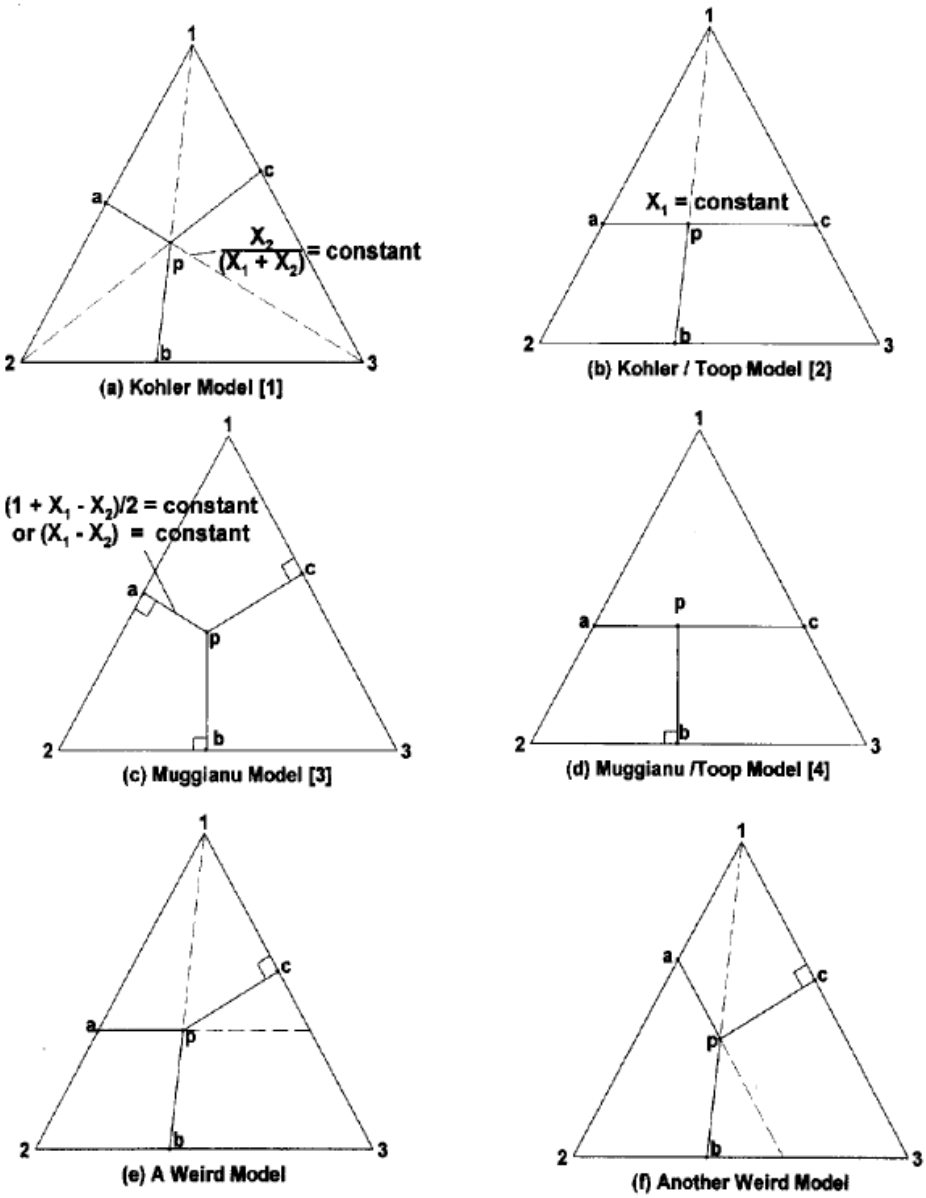

Figure 2.1. Geometric models for estimating ternary thermodynamic properties from the optimized binary phase diagrams [5].

Chapter 3. Key Phase Diagram Experiments and the Thermodynamic Optimizations of Binary ZnO-SnO_2, ZnO-SiO_2, and SnO_2-SiO_2 Systems

3.1. Introduction

Thermodynamic properties, phase diagrams, and chemical reactions of materials are crucial in understanding, developing, and optimizing new and existing material production processes. The knowledge of the Sn and Zn oxide containing multicomponent database (ZnO-SnO_2-SnO-SiO_2-CaO-Al_2O_3-Na_2O-Fe_2O_3-FeO- …) is essential in many industrial applications such as glassmaking, ceramics, steelmaking, and waste recycling [8–10]. Nevertheless, the phase diagrams of the ZnO and SnO_2 containing systems have not been well studied. This is due to the high vapor pressure and corrosivity of ZnO and SnO_2 that hinder the accurate thermodynamic study of such systems [11–13].

The purpose of the present study is to perform a critical evaluation and thermodynamic optimization of binary systems ZnO-SnO_2 and SnO_2-SiO_2. Because of the lack of phase diagram data of the ZnO-SnO_2 system and SnO_2-SiO_2 system available in literatures, key phase diagram experiments were

conducted to assist the thermodynamic optimization. The optimization results of the ZnO-SiO_2 system by Konar (unpublished work, 2018) is also presented.

3.2. Phase Diagram Experiment

3.2.1 Starting Materials

Starting materials were made of mechanical mixtures of SiO_2(Sigma Aldrich; 99.995% purity), SnO_2 (Sigma Aldrich; 99.9% purity), and ZnO (Sigma Aldrich; 99.99% purity). The purities of all the powders were all ensured by Bruker D8 Advance multi-purpose X-ray diffraction (XRD) analysis with Co-Kα source (λ = 1.79 Å) in Research Institute of Advanced Materials (RIAM) at Seoul National University (SNU). No significant foreign peaks that could be attributed to impurities were observed.

Because the vapor pressures of SnO_2 and ZnO are high at high temperatures, Zn_2SnO_4 was synthesized to alleviate this problem for the ZnO-SnO_2 system. Stoichiometric amounts of SnO_2 and ZnO were mixed in 2-3g batches in an alumina mortar filled with C_6H_{12}-cyclohexane (Sigma-Aldrich; 99.5% purity) for 15 minutes. The mixture of SnO_2 and ZnO were put in a platinum container with a lid and placed in a furnace at 1100°C for 10 hours to synthesize Zn_2SnO_4. XRD phase identification confirmed the synthesis of

stoichiometric Zn_2SnO_4.

All the samples with the proper proportions of SiO_2, SnO_2, and, Zn_2SnO_4 were made and stored in cyclohexane (Sigma Aldrich; 99.5% purity) to prevent any moisture or impurity pick-up. Before their usage, the samples were dried in a vacuum oven at 75°C. Then, the samples were put in sealed Pt capsules for the experiments at high temperature. The sealed capsules were used to prevent the volatization of SnO_2 and ZnO and any moisture contact of the samples. The Pt capsules were made from Pt tube (4 mm outer diameter and 0.5mm wall thickness), which were cut into ~10 mm long pieces. One side of the tube was first sealed using a tungsten electrode with a three-corner weld. After packing about 10~30 mg of the samples, the other side of the tube was also weld. The fineness of the weld was checked under an optical microscope before putting the capsules in the actual high temperature experiments. In addition, the Pt capsules were also sonicated in water for 10 minutes and the masses of the capsules before and after the sonication were compared to ensure the capsules were completely closed.

3.2.2. Differential Thermal Analysis

Differential thermal analysis (DTA) was performed using the Netsch STA 449 F5 equipment. Temperature calibrations were performed by the melting

temperatures or the polymorphic transitions of Ag_2SO_4, $BaCO_3$, $C_7H_6O_2$, $C_{12}H_{10}$, CsCl, $CaMgSi_2O_6$, K_2CrO_4, $KClO_4$, and $RbNO_3$. Experiments were conducted using sealed Pt capsules containing the samples inside DTA alumina crucible. The samples were heated to 1550ºC and cooled to 800ºC at 10ºC/min heating and cooling rate for two cycles in argon atmosphere with 20 mL/min flow rate. If necessary, the samples were reheated for a third cycle before being cooled down to room temperature. Thermo-gravimetric analysis (TGA) was simultaneously performed to confirm no mass loss by volatization. No bursting of the Pt capsules was observed after DTA experiments as well.

3.2.3. Quenching Experiments

Quenching experiments were conducted in KBM® vertical furnace equipped with $Pt_{30}Rh$-Pt_6Rh (type B) thermocouples. The sealed Pt capsules containing samples were hanged with a Pt wire and annealed at target temperatures. Then, the samples were quenched in water. Preliminary experiments were performed to evaluate the equilibration time. For samples containing SnO_2, bursting of the Pt capsules happened after 6hrs annealing above 1600ºC. This was expected due to the high vapor pressure and the corrosive nature of SnO_2. Thus, experiments at high temperatures were kept less than 6hrs to minimize the chance of the capsule bursting and the failure of the experiment. After the quenching experiments, no or negligible weight change of the Pt capsules

were confirmed.

3.2.4. Phase Characterizations

After the quenching experiments, the encapsulated samples were cast in epoxy and polished longitudinally using a diamond-based lapping oil as the polishing agent to avoid any moisture pick-up. Then, the samples were cleaned in an ultrasonic bath of cyclohexane, baked, and carbon coated. Phase characterization was performed using the backscattered electron (BSE) images from JEOL-8530F electron probe micro-analysis (EPMA) in the National Center for Inter-university Research Facilities (NCIRF) at SNU. The EPMA wavelength dispersive spectroscopy (WDS) phase compositional analyses were conducted using 15 kV accelerating voltage and 10 nA beam current. Beam diameter (3~10 μm) was set according to the sizes of each phase. Raw data were reduced with PRZ Armstrong algorithm employing standard samples of ZnO, SnO_2, and SiO_2, all provided by NCIRF. Part of the quenched samples were also ground and identified by XRD method. All peaks of the XRD were identified with powder diffraction files (PDF) from the International Center for Diffraction Data (ICDD) using Bruker AXS DIFFRAC.EVA software.

3.3. The ZnO-SiO_2 System

The ZnO-SiO_2 system was previously modeled by Konar (unpublished work, 2018) based on available phase diagram data and thermodynamic property data in literatures. The phase diagram of the ZnO-SiO_2 optimized by Konar is calculated in Figure 3.1 along with experimental data. Zn_2SiO_4 is the only intermediate compound that exists in the system and a miscibility gap in the SiO_2 rich region is present. The thermodynamic properties (c_p, enthalpy of formation of Zn_2SiO_4, and the activity of liquid) were all measured by many authors in the past. More data exist for the quenching experiment results analyzed by XRD, EPMA, EDS, etc [14–18].

In this work, the monotectic temperature ($L \rightarrow L + SiO_2$) was raised to 1689.5°C to better reproduce the ZnO-SnO_2-SiO_2 ternary phase diagram. Only slight modifications were made to the binary liquid parameter from Konar's optimization to reproduce this result (see Figure 3.1 and Table 3.5).

3.4. Study of the ZnO-SnO_2 System

3.4.1. Literature Review

No high temperature phase diagram data exists for the ZnO-SnO_2 system. Mihaiu et al. [19,20] studied the sub-solidus phase equilibria of the ZnO-SnO_2 system. In their studies, mixtures of ZnO and SnO_2 powders were annealed at

500, 600, 700, 800, 900, 1000, 1100, 1150, 1300, 1400, 1500ºC for 10hrs, and were cooled down to room temperature. After the experiments, the equilibrium phases were characterized by XRD analyses. They reported that SnO_2 and ZnO exist under 900ºC, and a three-phase assemblage of ZnO, SnO_2, and Zn_2SnO_4 exists at the temperatures between 900 and 1000ºC. Above the temperature, the phase diagram is divided into two phase regions of SnO_2 and Zn_2SnO_4 and ZnO and Zn_2SnO_4 without any other stoichiometric compound.

Gribchenkova et al. [2] performed a Knudsen cell effusion mass spectrometry experiment to measure the thermodynamic property of Zn_2SnO_4 in the temperature range between 1087 and 1187ºC. Based on the experimental data, they reported the standard Gibbs energy and standard enthalpy of formation of Zn_2SnO_4.

3.4.2. Key Phase Diagram Experiments

DTA analysis and multiple quenching experiments were conducted for the samples with 0.7 mol fraction SnO_2. The starting materials were made with a mixture of pre-synthesized Zn_2SnO_4 and SnO_2. DTA analysis up to 1550ºC revealed no phase transition until 1550ºC. Two experiments were conducted with open and closed Pt crucibles. Significant mass loss for sample in the open crucible was detected due to the volatilization of ZnO and SnO_2, as

shown in Figure 3.2. The same sample of 0.7 mol fraction SnO_2 was annealed at 1680°C for 1hr. Both XRD phase identification, BSE images (Figure 3.3), and EPMA compositional analysis (Table 3.2) revealed that solid Zn_2SnO_4 and SnO_2 exist at the temperature. Thus, it was concluded the solidus temperature of the ZnO-SnO_2 system in the SnO_2-rich region should be higher than 1680°C.

Series of experiments were designed to check the stability of Zn_2SnO_4 at temperature below 900°C. Reversibility of the reaction

$$2ZnO + SnO_2 \leftrightarrow Zn_2SnO_4$$

was investigated at 800 and 850°C. The starting stoichiometric mixture of ZnO and SnO_2 stayed as they were after 1wk annealing at 800°C. Zn_2SnO_4 stayed as it was after annealed for 1wk at 800°C. At 850°C, Zn_2SnO_4 was formed from the stoichiometric mixture of ZnO and SnO_2. Zn_2SnO_4 stayed as it was at 850°C. The experimental results of the Zn_2SnO_4 stability experiments are summarized in Table 3.3. If equilibrated for a longer period, it is expected from the experiments that the starting oxides, ZnO and SnO_2, should transform to Zn_2SnO_4. Due to the slow kinetics at 800°C, the formation or the decomposition of Zn_2SnO_4 cannot be confirmed in the present experiment.

3.4.3. Thermodynamic Optimization

Figure 3.4 shows the phase diagram optimized in the present study along with experimental data. The standard Gibbs energy of solid SnO_2 was taken from previous optimization by Yin (see details in the appendix, [21]), and the Gibbs energy of liquid SnO_2 was re-optimized according to the SnO_2 melting point newly estimated in the present study. The Gibbs energy of Zn_2SnO_4 was modeled based on the Knudsen cell effusion mass spectrometry data by Gribchenkova et al. [2] and the present experiment on the stability of Zn_2SnO_4. The thermodynamic properties of the stoichiometric phases in the ZnO-SnO_2 system is in Table 3.4.

There is no phase diagram experimental data related to the liquid of the ZnO-SnO_2 system. At least, the present experiment confirmed that the liquidus between Zn_2SnO_4 and SnO_2 should be higher than 1680°C. Considering that SnO_2 behaves as a network former (acidic component in oxide system), the interaction between ZnO and SnO_2 in the liquid state was assumed to be like that of ZnO and SiO_2. As can be seen in Figure 3.4., the phase diagram of the ZnO-SnO_2 system in the present study is very similar to that of the ZnO-SiO_2 system in Figure 3.1. Two model parameters were used to create a large miscibility gap in the SnO_2-rich region. The $\Delta g_{Zn^{2+}-Sn^{2+}}$ in the present study are listed in Table 3.5.

3.5. Study of the SnO_2-SiO_2 System

The successful phase equilibrium study of the SnO_2-SiO_2 system can be hindered by many obstacles. First, the volatility of SnO_2 is high as it decomposes rapidly to $SnO_{(g)}$ and $O_{2(g)}$ above 1200°C [12]. Moreover, Sn oxide is corrosive. Thus, the good refractory crucible material for the experiment is critical. Because of the corrosivity and the high vapor pressure, long time phase diagram experiments for the SnO_2 containing system at high temperature are very difficult. The viscosity of SiO_2 containing slag is high, so the equilibration for the SnO_2-SiO_2 system would take a long time. The contradicting experimental requirements make the accurate phase diagram study of the SnO_2-SiO_2 system to be very challenging.

3.5.1. Literature Review

In 2018, Yin [21] utilized a double closed crucible for the phase diagram study of the SnO_2-SiO_2 system to minimize the volatile loss of SnO_2. A Re inner crucible was made of 0.0127mm Re foil, coiled three times to retain a cylindrical shape of 3.5mm length and 2.5mm diameter, with a wall thickness of 0.0381mm. The outer crucible consisted of Pt capsules 15mm in length, 2.873mm in inner diameter, and 3mm outer diameter. However, this experimental set up was insufficient to withhold the high vapor pressure of

SnO_2. Therefore, above 1600°C, experiment could not be held for more than 15 minutes which was insufficient to reach equilibrium state. Although she could not obtain full equilibrium, from the change of the morphology of starting solid SnO_2 and SiO_2, she concluded a liquid miscibility gap in the SnO_2-rich region and eutectic of SnO_2 and SiO_2 in the SiO_2-rich region. The eutectic and monotectic temperatures were set at 1500~1510°C and 1625~1650°C, respectively. No intermediate stoichiometric oxide phase was detected between SnO_2 and SiO_2, and no significant mutual solubilities between solid SnO_2 and SiO_2 were detected. No other phase diagram study has been attempted in the SnO_2-SiO_2 system.

3.5.2 Key Phase Diagram Experiments

To overcome the rupture of sealed Pt crucible by high vaporization of SnO_2, Pt tubes (4 mm outer diameter and 0.5mm wall thickness) were used in the phase diagram study. Pt tube with thicker wall could withstand the vapor pressure and corrosivity of SnO_2 up to 6hrs over 1600°C. The starting materials of the experiment were consisted of $X_{SnO_2} = 0.15$ and $X_{SnO_2} = 0.50$. Both DTA experiment and annealing experiments were performed and their results are summarized in Table 3.6 and 3.7. The results of the DTA analyses for both samples revealed that no phase transition from solid SnO_2 and SiO_2 occurred until 1550°C. The samples with the composition of

$X_{SnO_2} = 0.15$ and $X_{SnO_2} = 0.50$ were equilibrated at 1570~1600, 1650, and 1675~1680°C to check the formation of liquid phase in this system. For samples with $X_{SnO_2} = 0.50$, at 1600°C and 1650°C, both solid SiO_2 and SnO_2 phases were found by XRD phase identification at 1600 and 1650°C after equilibration for 3hrs. The sample annealed at 1680°C for 3hrs showed no solid SiO_2 peak from XRD analysis. Unfortunately, no broad peak for glass phase was detected in XRD analysis too. Similar results were obtained from the samples with the composition of $X_{SnO_2} = 0.15$. Both crystal peaks of SiO_2 and SnO_2 were identified from the sample annealed at 1600 and 1650°C. At 1675°C, SiO_2 crystal peak disappeared, and an existence of a glass phase could be clearly identified (see Figure 3.5). Based on these experimental results, it can be concluded that the eutectic reaction for L → SiO_2 + SnO_2 occurs at 1650~1675°C, and the eutectic composition is $X_{SnO_2} < 0.15$.

EPMA compositional analyses were also conducted to identify the phases in the equilibrated samples. Figure 3.6 shows the BSE images of the samples with $X_{SnO_2} = 0.15$ annealed at 1650 and 1675°C. Even though liquid (SiO_2-rich) was formed at 1675°C, the enlargement of solid SnO_2 did not happen even after 6hr due to the very high viscosity of SiO_2-rich liquid phase. According to the EPMA results, a glass phase contains only 1.1mol% SnO_2. If the sample is equilibrated for a longer time to reach full equilibrium, there is a chance that the SnO_2 content in liquid phase would become higher.

3.5.3. Thermodynamic Optimization

From the present experiment, it is confirmed that there is no intermediate compound between SnO_2 and SiO_2. To explain the eutectic reaction for liquid → SnO_2+SiO_2 at 1650~1675°C and eutectic liquid with nearly pure SiO_2 composition, a wide liquid miscibility should be assumed in the SiO_2-SnO_2 system.

To reproduce the present experimental results, the binary MQM parameter $\Delta g_{Si^{4+}-Sn^{4+}}$ was optimized (see Table 3.5). The calculated phase diagram of the SnO_2-SiO_2 system from the present optimization is presented in Figure 3.7 along with experimental data. According to the present optimization, the eutectic temperature is 1674.7°C and the eutectic composition is X_{SiO_2} =0.974. The predicted monotectic temperature of L (X_{SiO_2} = 0.0428) → L (X_{SiO_2} = 0.957) + SnO_2 is 1734.4°C.

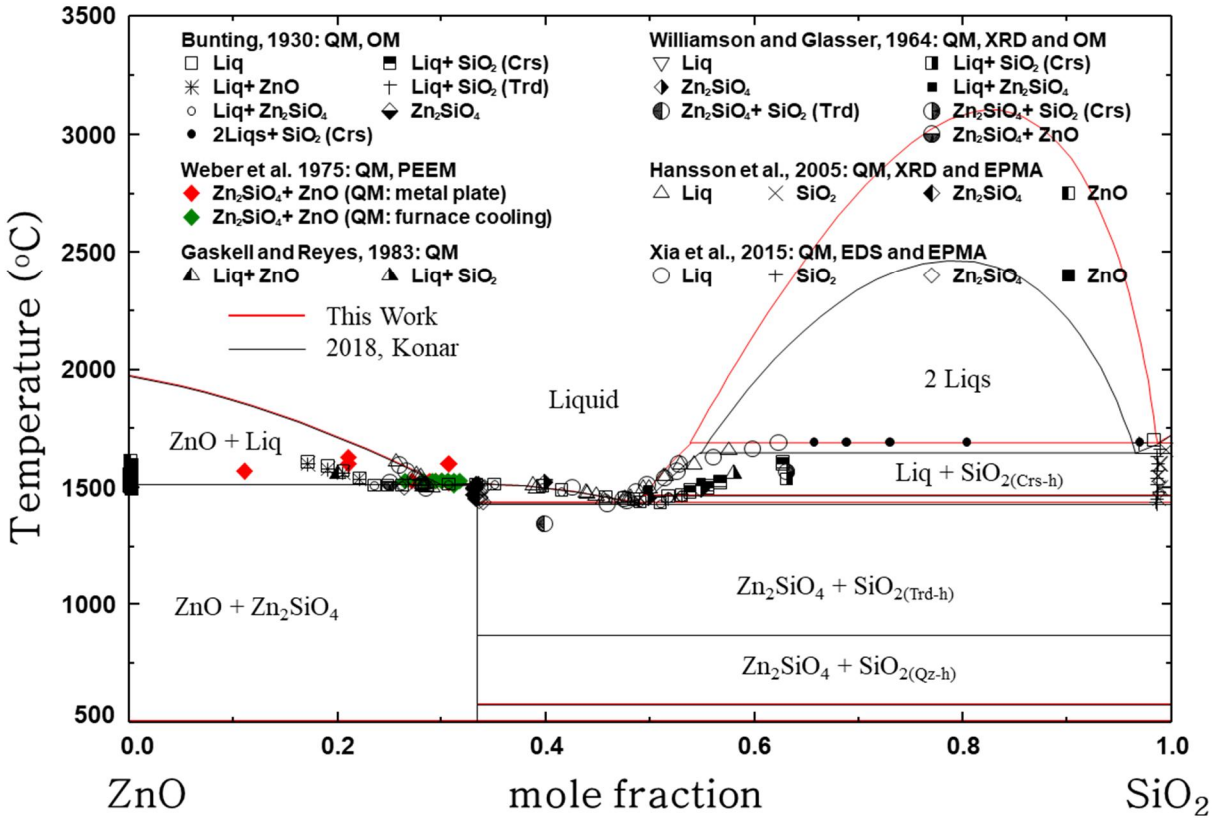

Figure 3.1. Phase diagram of the ZnO-SiO_2 system optimized by Konar (unpublished work) and re-optimized in the present work along with experimental data.

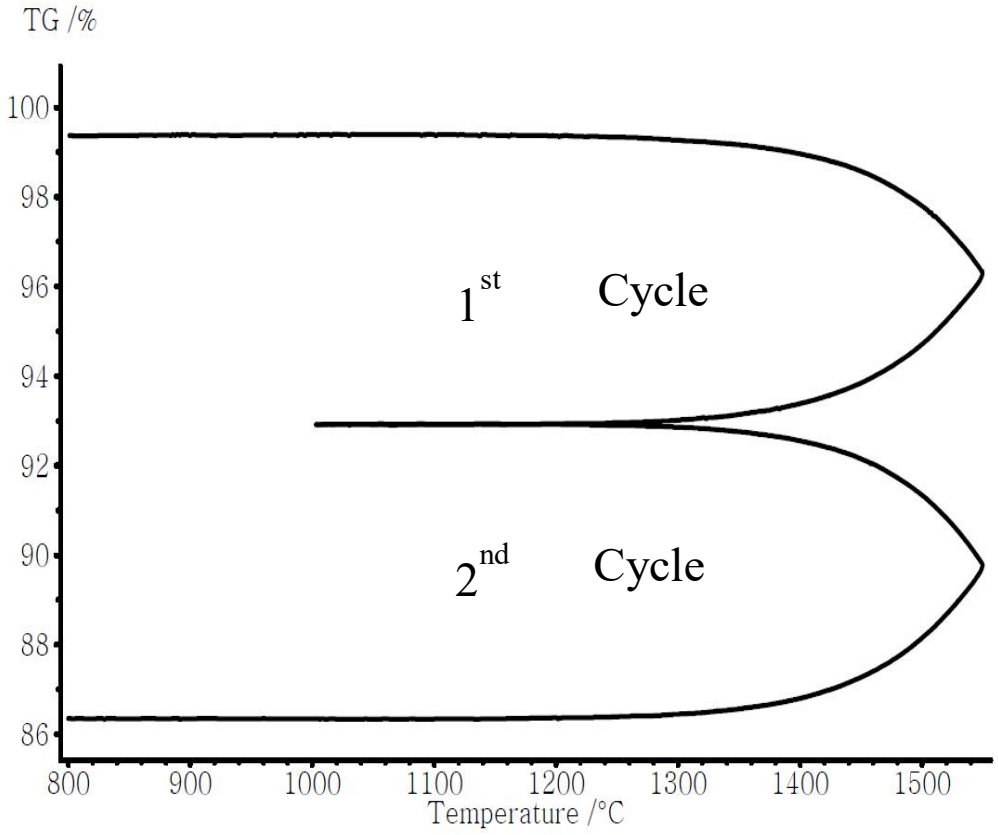

Figure 3.2. TG curve for the weight loss of DTA II experiment using an open crucible.

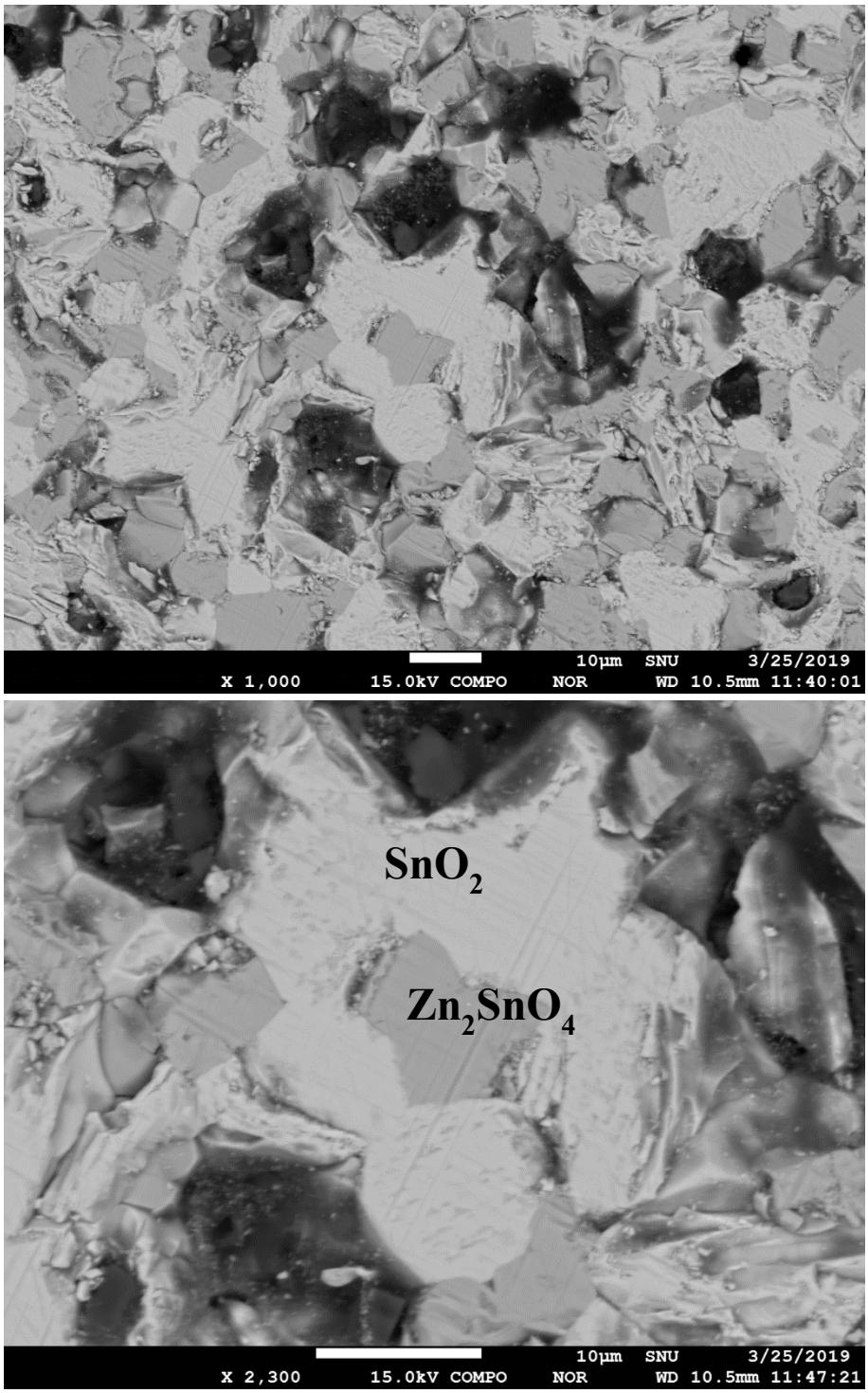

Figure 3.3. Microstructure of stating materials with X_{SnO_2}= 0.7, equilibrated at 1680ºC for 1 hr (Sample II in Table 3.2).

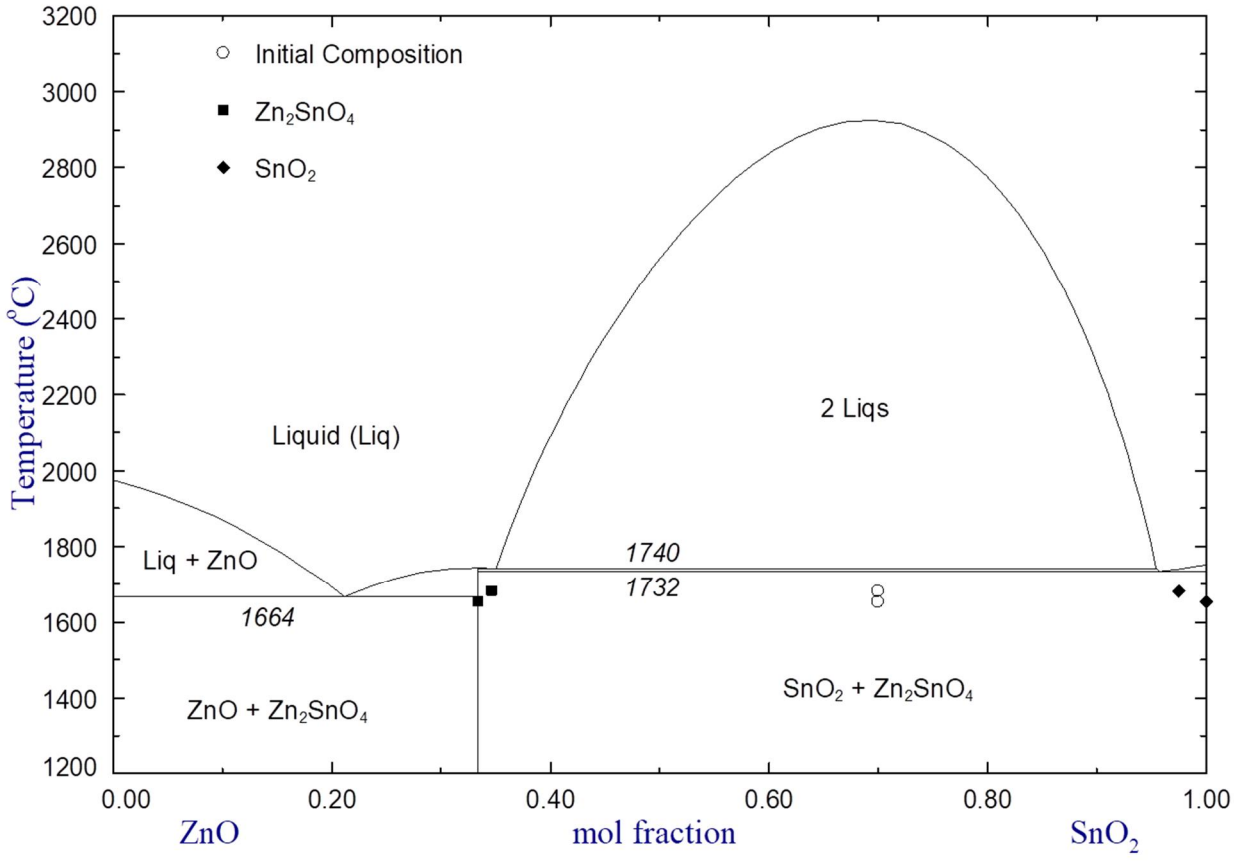

Figure 3.4. The optimized phase diagram of the ZnO-SnO_2 system in air along with present experimental data.

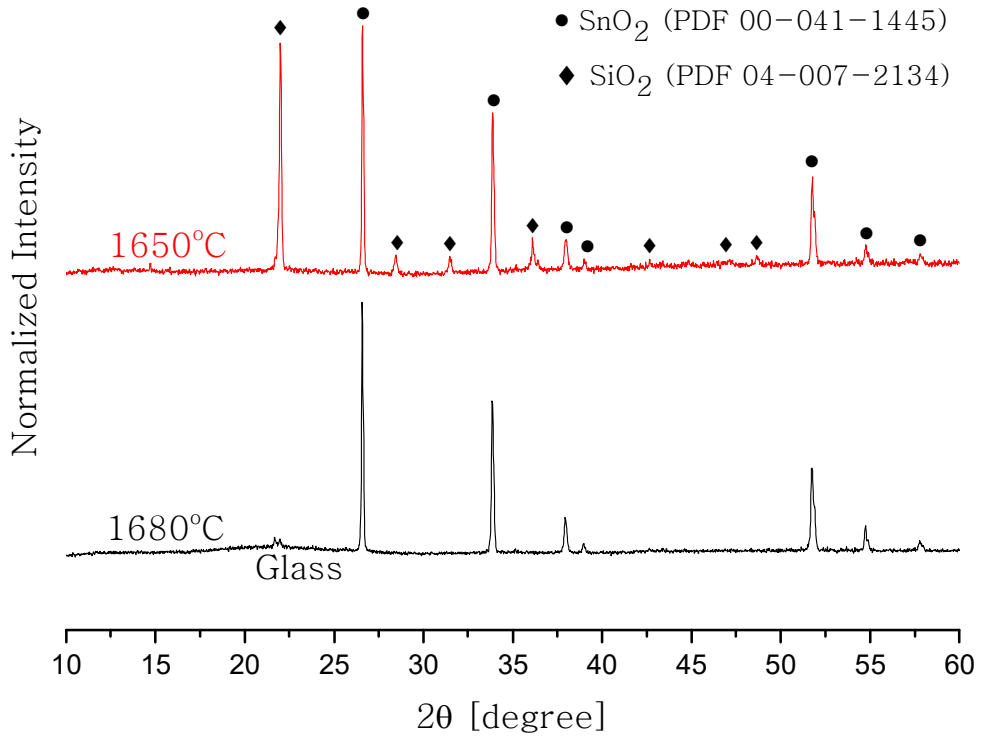

Figure 3.5. XRD phase analysis of the quenched samples ($X_{SnO_2} = 0.15$) after equilibration at 1650°C and 1675°C for 3hrs.

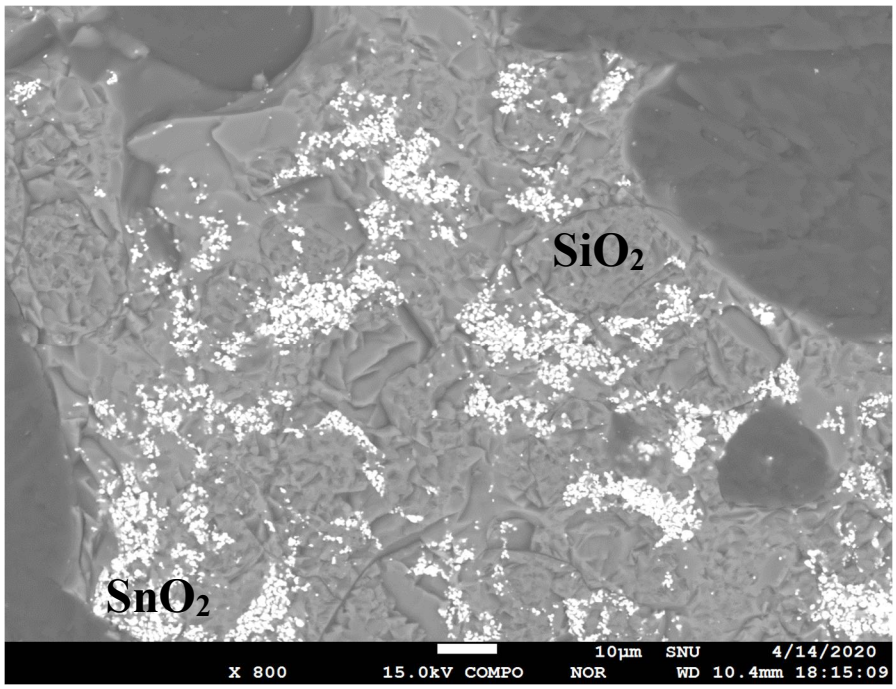

a)

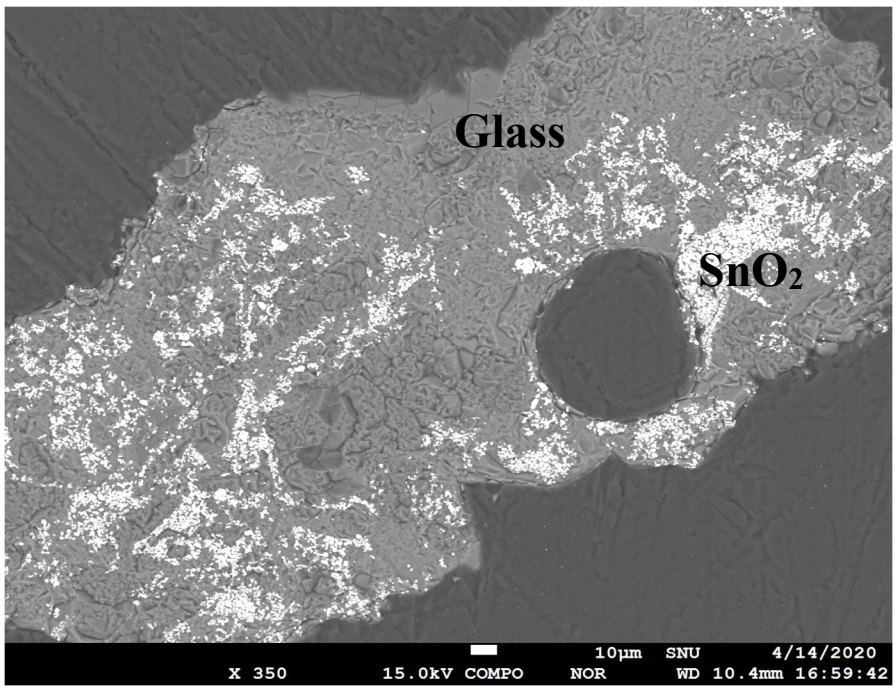

b)

Figure 3.6. Microstructure of the quenched samples ($X_{SnO_2} = 0.15$) after equilibration at a) 1650ºC and b) 1675ºC for 3hrs.

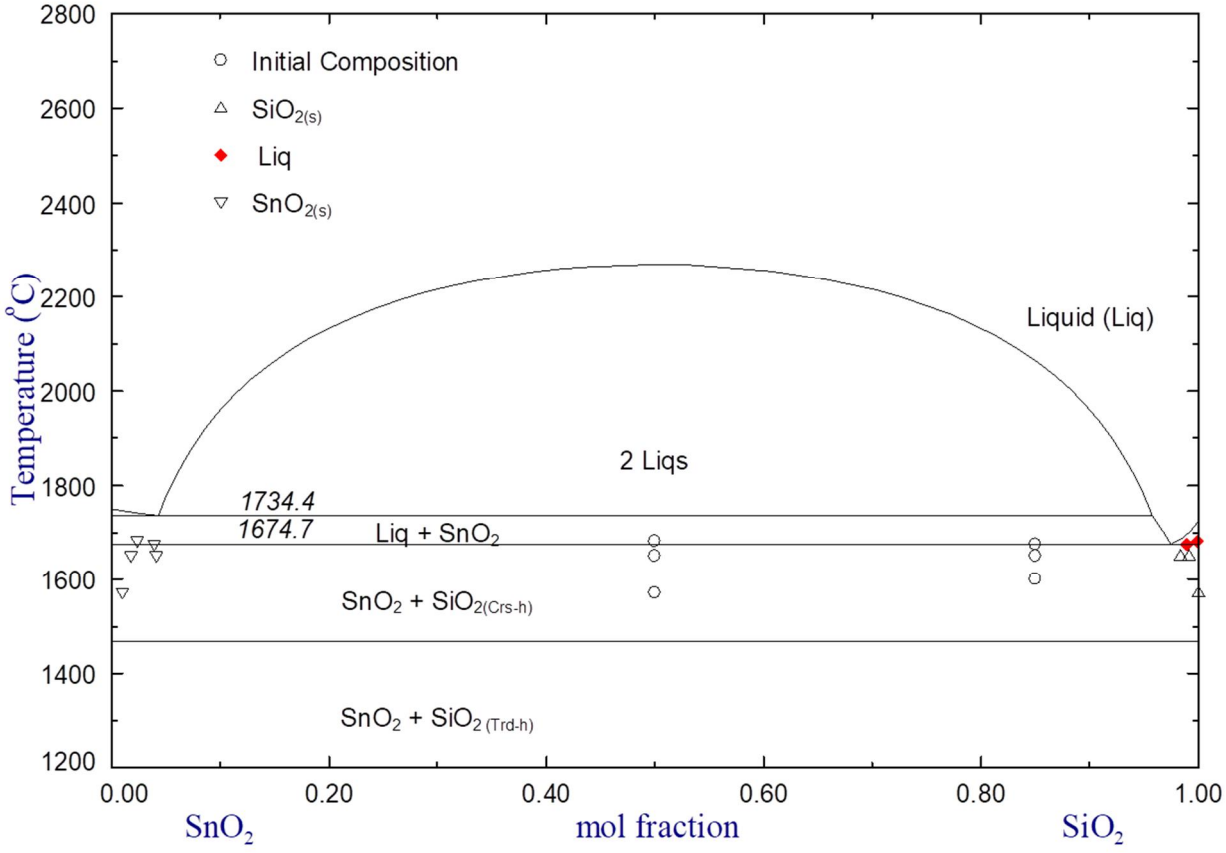

Figure 3.7. The optimized phase diagram of the SnO_2-SiO_2 system along with present experimental data.

Table 3.1. Summary of the DTA experiments in the binary ZnO-SnO_2 system.

Sample	Starting Composition (mol fr. SnO_2)	Temperature (ºC)	Rate (ºC/min)	Transition	Comments
DTA I	1.0	25-1550	10	None	
DTA II	0.7	25-1550	10	None	Open crucible*
DTA III	0.7	25-1550	10	None	Closed crucible

* Significant mass loss.

Table 3.2. Summary of the equilibration experiments in the binary ZnO-SnO_2 system. Starting materials were all made from a mixture of Zn_2SnO_4 and SnO_2.

Sample	Starting Composition* (mol fr. SnO_2)	Temperature (°C)	Duration (hr)	Phases (XRD)	EPMA Analysis	
					ZnO (mol fr.)	SnO_2 (mol fr.)
I	1.0	1650	1	$SnO_{2(s)}$	Not analyzed by EPMA	
II	1.0	1680	1	$SnO_{2(s)}$		
III	0.7	1650	1	$SnO_{2(s)}$		
				$Zn_2SnO_{4(s)}$		
IV	0.7	1680	1	$SnO_{2(s)}$	0.0254	0.975
				$Zn_2SnO_{4(s)}$	0.654	0.346

* Starting materials were all made from a mixture of Zn_2SnO_4 and SnO_2.

Table 3.3. Summary of the experimental results for the decomposition of Zn_2SnO_4.

Sample	Starting Composition (mol fr. SnO_2)	Starting Materials	Temperature (ºC)	Duration (Week)	Phases (XRD)
I	0.33	ZnO, SnO_2	800	1	$ZnO_{(s)}$, $SnO_{2(s)}$
II	0.33	Zn_2SnO_4	800	1	$Zn_2SnO_{4(s)}$
III	0.33	ZnO, SnO_2	850	2	$ZnO_{(s)}$, $SnO_{2(s)}$, $Zn_2SnO_{4(s)}$
IV	0.33	Zn_2SnO_4	850	2	$Zn_2SnO_{4(s)}$

Table 3.4. Summary of thermodynamic properties of the stoichiometric phases in the ZnO-SnO_2 and SnO_2-SiO_2 systems.

Phase	$\Delta H^{o}_{298.15}$ (kJ/mol)	$S^{o}_{298.15}$ (J/mol K)	c_p (J/mol K)	Reference
$SnO_{2(s)}$	-577.63	49.01	$76.041 + 0.0073622T - 2223867T^{-2} + 7.69E - 10T^{2}$ $(25 - 1630°C)$	[21]
$SnO_{2(l)}$	-553.06	40.52	92 $(1630 - 4127°C)$	This Work
$ZnO_{(s)}$	-350.46	43.64	$48.2415 + 0.006795T - 103768354.688T^{-3} - 91.5474T^{-0.5}$ $(25 - 1975°C)$ 60.668 $(1975 - 2227°C)$	[22]
$ZnO_{(l)}$	-296.07	67.83	$48.2415 + 0.006795T - 103768354.688T^{-3} - 91.5474T^{-0.5}$ $(25 - 1975°C)$ 60.668 $(1975 - 2227°C)$	[22]
$SiO_{2(Quartz\ I)}$	-910.67	41.46	$80.0120 - 3546683.9989T^{-2} - 240.2760T^{-0.5} + 491568369.44T^{-3}$ $(25 - 100°C)$ $80.0120 + 0.008440T - 3546683.9989T^{-2} - 4.5213E - 5T^{2} + 6.0550E - 8T^{3} - 240.2760T^{-0.50} + 491568369.44T^{-3}$ $(100 - 575°C)$ 0.04184 $(575 - 577°C)$	[23,24]
$SiO_{2(Quartz\ II)}$	-908.63	44.21	$80.0120 - 3546683.9989T^{-2} - 240.2760T^{-0.5} + 491568369.44T^{-3}$ $(25 - 1722°C)$	[23,24]

			$85.772\ (1772-2727℃)$	
$SiO_{2(Tridymite)}$	-907.05	45.52	$75.3727-5958095.0776T^{-2}-958246122.88T^{-3}\ (25-1718℃)$	[23,24]
$SiO_{2(Cristobalite)}$	-906.38	46.03	$83.5136-2455359.9821T^{-2}-374.6930T^{-0.50}+280072194.424T^{-3}\ (25-1723℃)$	[23,24]
			$85.772\ (1723-2727℃)$	
$SiO_{2(l)}$	-896.796	50.829	$85.5136-2455359.9821T^{-2}-374.6930T^{-0.50}+280072194.424T^{-3}\ (25-1723℃)$	[23,24]
			$85.772\ (1723-2727℃)$	
Zn_2SnO_4	-1293.20	140.10	$172.5240+0.02095T-2223867T^{-2}+7.69E-10T^{2}-207536709.376T^{-3}-183.0948T^{-0.50}\ (25-1630℃)$	[2], This Work
			$185.9229+0.01359T-207536709.376T^{-3}-183.0948T^{-0.50}\ (1630-1975℃)$	
			$210.7759\ (1975-2227℃)$	

Table 3.5. The optimized MQM parameters for liquid phase in the present study (J/mol).

Solution	Δg_{AB}
ZnO-SiO2	$\Delta g_{Zn^{2+}-Si^{4+}} = -22000 - 7000X_{Zn^{2+}-Zn^{2+}} + 62000X^{2}_{Si^{4+}-Si^{4+}} + 37000X^{5}_{Si^{4+}-Si^{4+}}$
ZnO-SnO2	$\Delta g_{Zn^{2+}-Sn^{4+}} = -15000 + 65000X_{Sn^{4+}-Sn^{4+}} + 35000X^{3}_{Sn^{4+}-Sn^{4+}} - 5000X_{Zn^{2+}-Zn^{2+}}$
SiO2-SnO2	$\Delta g_{Sn^{4+}-Si^{4+}} = 54700$

Table 3.6. Summary of the DTA experiment for the binary SnO_2-SiO_2 system.

Sample	Starting Composition (mol fr. SnO_2)	Temperature (ºC)	Rate (ºC/min)	Transition
DTA I	0.15	25-1550	10	None
DTA II	0.5	25-1550	10	None

Table 3.7. Summary of the equilibration experiments for the binary SnO_2 -SnO_2 system.

Sample	Starting Composition (mol fr. SnO_2)	Temperature (°C)	Duration (hr)	Phases (XRD)	EPMA Analysis	
					SnO_2 (mol fr.)	SiO_2 (mol fr.)
I	0.5	1570	3	$SnO_{2(s)}$	0.991	0.00930
				$SiO_{2(s)}$	0.000398	0.999
II	0.5	1650	3	$SnO_{2(s)}$	0.973	0.0275
				$SiO_{2(s)}$	0.00684	0.993
III	0.5	1680	3	$SnO_{2(s)}$	0.976	0.0237
				Glass	0.000820	0.999
IV	0.15	1600	3	$SnO_{2(s)}$ $SiO_{2(s)}$	Unstable EPMA Total	
V	0.15	1650	3	$SnO_{2(s)}$	0.966	0.0343
				$SiO_{2(s)}$	0.0124	0.988
VI	0.15	1650	12	$SnO_{2(s)}$	0.959	0.0411
				$SiO_{2(s)}$	0.00902	0.991
VII	0.15	1675	3	$SnO_{2(s)}$	0.961	0.0388
				Glass	0.0105	0.989

Chapter 4. A coupled Phase Diagram Experiment and Thermodynamic Optimization of the ZnO-SnO_2-SiO_2 System

4.1 Introduction

The thermodynamic database for the Sn oxide containing multicomponent system SnO_2-SnO-ZnO-SiO_2-CaO-Al_2O_3-Fe_2O_3-FeO-… is essential in various industrial applications including ceramics, glass, recycling, and geochemistry [8–10,25]. The present optimization is part of an effort to create a larger thermodynamic database that can be utilized for various practical applications. In this study, a coupled phase diagram experiment and optimization of the ZnO-SnO_2-SiO_2 system was conducted to understand the thermodynamic properties and the phase relationships of the ternary system.

4.2 Literature Review

No data could be found for the phase diagram or thermodynamic study on this ternary ZnO-SnO_2-SiO_2 system.

4.3 Phase Diagram Experiments

4.3.1 Materials Preparation

Because both ZnO and SnO_2 have high vapor pressure at high temperatures, special care was taken for the starting materials in the present phase diagram experiments. Starting materials were prepared in two ways. In the first method, pre-synthesized Zn_2SnO_4 was used. Zn_2SnO_4 was pre-synthesized by annealing stoichiometric amounts of ZnO and SnO_2 at 1100°C for over 10hrs. The target starting compositions were prepared in an agate mortar using Zn_2SnO_4, ZnO, SnO_2, and SiO_2. The mixtures were stored in a cyclohexane liquid and dried in vacuum oven at 75°C prior to their usages. The second method employed a pre-annealing stage. The mechanical mixture of ZnO, SnO_2, and SiO_2 for a target starting composition was put in a platinum crucible and annealed overnight in a box furnace at 1100°C. To confirm negligible weight loss of SnO_2 and ZnO by volatization, the sample weights before and after annealing were compared. These pre-annealed samples were cooled down to room temperature and used for the staring materials for the phase diagram experiment.

For the main DTA and quenching experiments, the starting materials were put in sealed Pt capsules. Pt capsules were made from Pt tube (4 mm outer diameter and 0.5mm wall thickness), which were cut into ~10 mm long pieces. One side of the tube was first sealed using a tungsten electrode with a three-

corner weld. After packing about 10~30 mg of the samples, the other side of the tube was also weld. The integrity of the weld was checked under an optical microscope before utilizing the capsules in the actual DTA and quenching experiments. In addition, the Pt capsules were also sonicated in water for 10 minutes and the mass of the capsules before and after the sonication were compared. The reason for employing the sealed Pt capsules was also to minimize the evaporation of ZnO and SnO_2 during the high temperature experiments and prevent any moisture contact of samples.

4.3.2 Differential Thermal Analysis

Differential thermal analysis (DTA) was performed using the Netsch STA 449 F5 equipment. Temperature calibrations were performed by the melting and the polymorphic transition temperatures of Ag_2SO_4, $BaCO_3$, $C_7H_6O_2$, $C_{12}H_{10}$, CsCl, $CaMgSi_2O_6$, K_2CrO_4, $KClO_4$, and $RbNO_3$. Sealed Pt capsules containing the samples were put inside DTA alumina crucible, and samples were heated to 1550ºC and cooled at 10ºC/min to 800ºC for three cycles in argon atmosphere with 20 mL/min flow rate before being cooled down to room temperature. No bursting of the Pt capsules after the DTA experiments were observed.

Two DTA experiments were conducted for two samples to find the ternary

eutectic temperatures in the ZnO-rich region and the SiO_2-rich region, respectively, of the ZnO-SnO_2-SiO_2 system (the starting compositions were 0.2ZnO-0.4SnO_2-0.4SiO_2 and 0.8ZnO-0.1SnO_2-0.1SiO_2). The ternary eutectic temperatures determined in the DTA experiments were 1424.6°C (high SiO_2 region) and 1464.8°C (high ZnO region). Summary of the DTA experiments and raw data are presented in Table 4.1 and Figure 4.1.

4.3.3 Quenching Experiments

Series of equilibrium and quenching experiments were conducted above 1200°C to accurately determine the phase diagram of ZnO-SnO_2-SiO_2 system. All the experimental results are summarized in Table 4.2.

4.3.3.1 Phase Diagram at Sub-solidus Temperature (1200°C)

To find the sub-solidus phase equilibria of the ZnO-SnO_2-SiO_2 system, three samples were equilibrated at 1200°C for 48hrs and quenched in water. The quenched samples were pulled out from the platinum crucible and ground in an agate mortar. The phase identifications of the ground samples were conducted by X-ray diffraction (XRD) method with Co-Kα source (λ = 1.79 Å) at Research Institute of Advanced Materials (RIAM) in Seoul National University (SNU). All peaks of the XRD were identified with powder

diffraction files (PDF) from the International Center for Diffraction Data (ICDD) using Bruker AXS DIFFRAC.EVA software.

ZnO, Zn_2SnO_4, and Zn_2SiO_4 solid phases were found in equilibrium for the sample of $0.8ZnO\text{-}0.1SnO_2\text{-}0.1SiO_2$ in mol fraction. For the sample of $0.6ZnO\text{-}0.2SnO_2\text{-}0.2SiO_2$, SiO_2, Zn_2SnO_4, and Zn_2SiO_4 phases were found. Lastly, for the sample of $0.2ZnO\text{-}0.4SnO_2\text{-}0.4SiO_2$, XRD phase analysis showed the assemblage of SnO_2, SiO_2, and Zn_2SnO_4. No ternary phase was found.

4.3.3.2 Ternary Eutectic Compositions

To find the ternary eutectic compositions for two eutectic reactions identified in the DTA experiments (see Table 4.1), quenching experiments were performed. The same two starting materials used for the DTA experiments were employed and equilibrated at 1450ºC and 1500ºC, which were about 25~35ºC above the eutectic temperatures. The quenched samples were analyzed using XRD and electron probe micro-analysis (EPMA). The back scattered electron (BSE) images results of the quenched samples are presented in Figure 4.2.

For the sample with the starting composition of $0.2ZnO\text{-}0.4SnO_2\text{-}0.4SiO_2$

equilibrated at 1450°C for 1 hr, solid SnO_2 and SiO_2, and a glass phase were found (see Figure 4.2 a). The composition of the glass phase was analyzed to be $0.512ZnO\text{-}0.021SnO_2\text{-}0.467SiO_2$ from EPMA. This should be close to the eutectic composition for the reaction of L → SnO_2 + SiO_2 + Zn_2SnO_4 at 1424.6°C. The other eutectic composition is close to $0.688ZnO\text{-}0.037SnO_2\text{-}0.275SiO_2$ for the L → ZnO + Zn_2SnO_4 + Zn_2SiO_4 reaction at 1464.8°C (see Figure 4.2 b).

4.3.3.3 Isothermal Phase Diagram at 1600°C

Isothermal phase diagram at 1600°C was investigated using multiple quenching experiments. The resultant phase relationships at various sections of the phase diagram are summarized in Table 4.2 and presented in Figure 4.3. In the sample of $0.2ZnO\text{-}0.4SnO_2\text{-}0.4SiO_2$ equilibrated at 1600°C for 6hrs, SiO_2 and SnO_2 crystal, and glass phases were found. Glass phase showed an anomaly with small "pore" like SiO_2 rich precipitates identified by EPMA mapping (Figure 4.4). In the sample of the same composition equilibrated at 1450°C for 1 hr, the glass phase did not have such anomaly.

Both XRD phase identification and EPMA analysis revealed solid SnO_2 and glass phase as equilibrium phases in the sample of $0.4SnO_2\text{-}0.35SnO_2\text{-}0.25SiO_2$ at 1600°C. Micro-precipitates (about the size of 0.5μm) like those

of Figure 4.4 with high SiO_2 composition were formed compactly in the glass phase. The EPMA total of the glass phase was only 92~94, so an accurate composition of the glass could not be determined.

For the quenching experiments at the starting compositions of 0.5ZnO-0.45SnO_2-0.05SiO_2 (Figure 4.3 c) and 0.6ZnO-0.3SnO_2-0.10SiO_2 (Figure 4.3 d), a glass phase, $SnO_{2(s)}$, and $Zn_2SnO_{4(s)}$were found in the BSE images. However, quenched crystal Zn_2SiO_4 dendrite was also found in XRD analysis. The glass phase with the dendritic structure had the average composition of 0.637ZnO-0.108SnO_2-0.255SiO_2. The sample with the starting composition of 0.63ZnO-0.05SnO_2-0.32SiO_2 showed only a single glass phase (Figure 4.3 e). The sample in the ZnO-rich region (0.8ZnO-0.1SnO_2-0.1SiO_2) showed the assemblage of solid ZnO and Zn_2SnO_4, and glass phases (Figure 4.3 f). Due to the low viscosity of the melt, the quenched crystals of Zn_2SiO_4 dendrites were well developed.

4.3.3.4. Quenching Experiments Above 1650°C

The sample of 0.2ZnO-0.4SnO_2-0.4SiO_2 was equilibrated at 1650 and 1675°C for 20 and 3 hrs, respectively. The phase analysis by XRD for the 1650°C sample showed the existence of solid SnO_2 and SiO_2 and glass (Figure 4.4 a) while only solid SnO_2 and glass were detected in the sample at 1675°C (Figure

4.5 b). Unfortunately, the glass compositions could not be accurately quantified by EPMA because of the abnormal precipitates forming.

For the sample of $0.4SnO_2$-$0.35SnO_2$-$0.25SiO_2$ (Figure 4.5 c), only $SnO_{2(s)}$ and glass phase were found. However, the composition of the glass phase could not be accurately quantified because of the precipitates. ZnO, Zn_2SnO_4, and glass phase formed for the phase equilibrium of sample at $0.6ZnO$-$0.3SnO_2$-$0.1SiO_2$ (Figure 4.5 d).

4.3.3.5. Others

The EPMA composition results of all solid phases were analyzed. Negligible solubilities of ZnO and SiO_2 in SnO_2 were found. Similarly, the solubilities of ZnO and SnO_2 in SiO_2 was also negligible. On the other hand, ZnO solid phase contained 0.06~0.07 of SnO_2 and 0.01~0.03 of SiO_2 ($0.8ZnO$-$0.1SnO_2$-$0.1SiO_2$ sample). This is rather surprising result. Further experimental study would be required to accurately quantify the solubility and dissolution mechanism.

4.4. Thermodynamic Modeling

To reproduce all experimental phase diagram data in the present study, the

Gibbs energy of the liquid phase was optimized. In the present thermodynamic optimization, all solid phases were assumed to be stoichiometric compounds. No ternary compounds were found in the present study. The standard Gibbs energies of solid and liquid compounds were taken from the previous optimization in chapter 3 without any modifications.

The Gibbs energy of the ternary ZnO-SnO_2-SiO_2 liquid oxide solution was described using the Modified Quasi-chemical Model (MQM). The binary MQM parameters can be utilized to predict the Gibbs energy of the ternary liquid solution using the geometric interpolation technique. In the present ZnO-SnO_2-SiO_2 system, Toop interpolation technique with ZnO as the asymmetric component was employed because ZnO is a basic oxide and SnO_2 and SiO_2 are acidic oxides in the ternary solution.

The prediction from binary parameters give reasonable result for the ternary phase diagram. However, to better reproduce the experimental phase diagram data in the present study, two ternary parameters were introduced.

$$q^{201}_{Zn^{2+}Si^{4+}(Sn^{4+})} = 22000 \ \text{J/equiv}$$

$$q^{013}_{Sn^{4+}Zn^{2+}(Si^{4+})} = -51544 + 8.5714 \ \text{T} \ \text{J/equiv}$$

where J/equiv stands for J/equivalent site fraction.

The liquid projection of the ZnO-SnO_2-SiO_2 system was predicted (Figure 4.6 and Table 4.3) from the present thermodynamic optimization results. Figure 4.7 shows the isothermal phase diagrams calculated in the present study in comparison with experimental results.

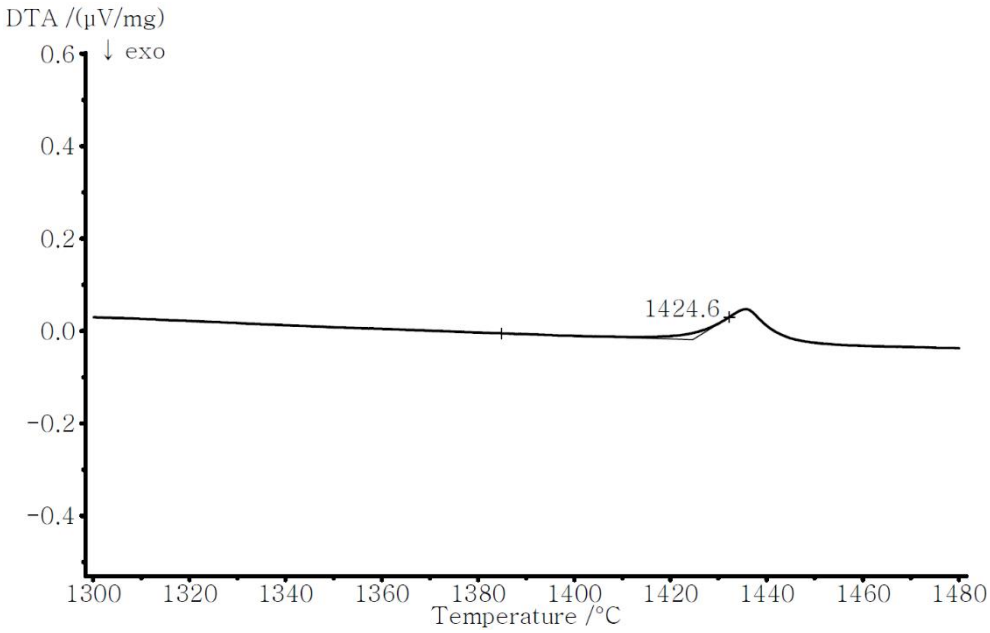

a)

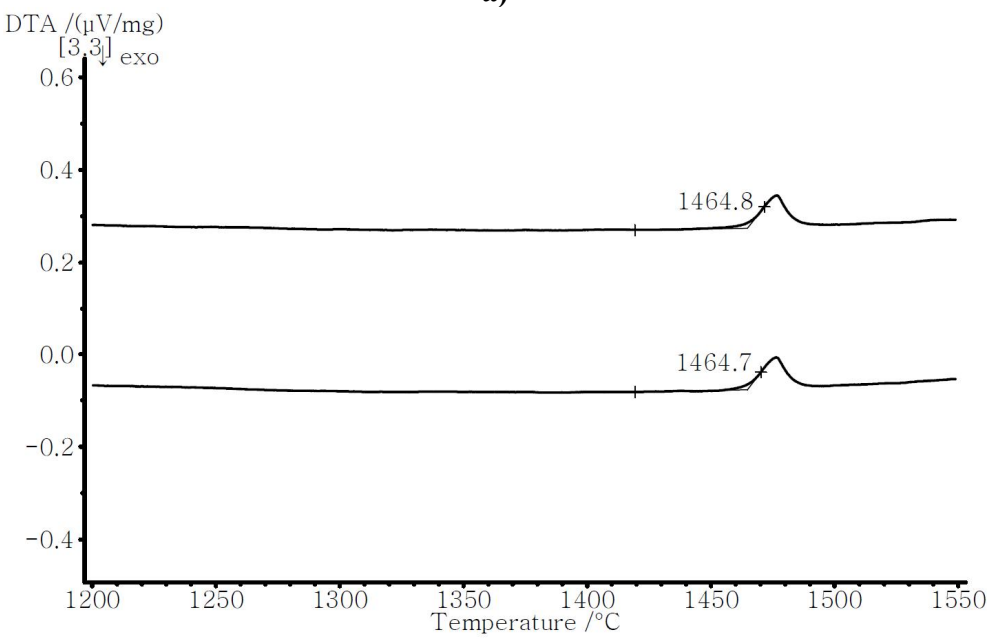

b)

Figure 4.1. Results of DTA for the samples in the ternary ZnO-SnO_2-SiO_2 system. a) sample I, and b) II of Table 4.1.

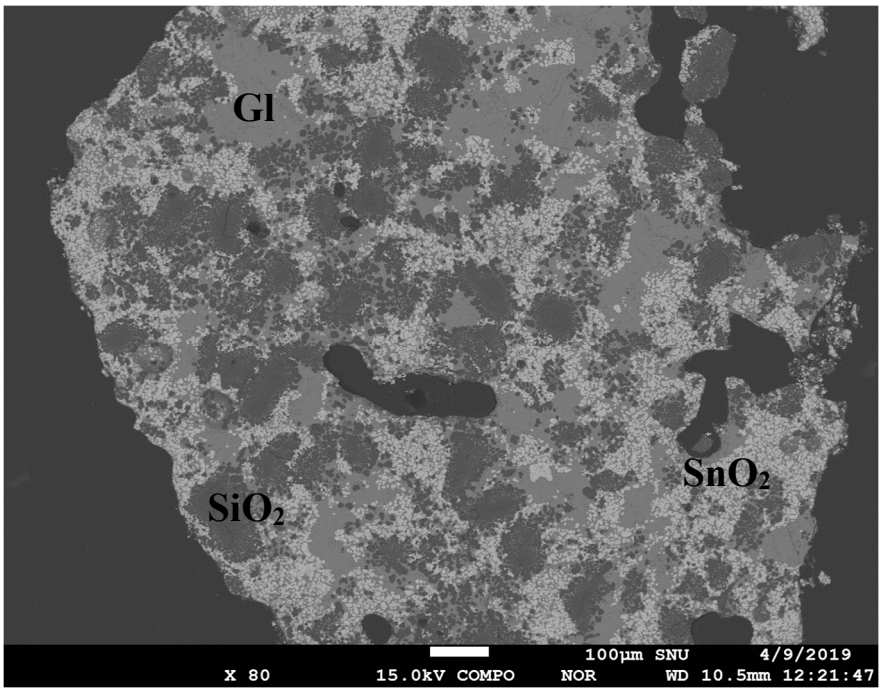

a)

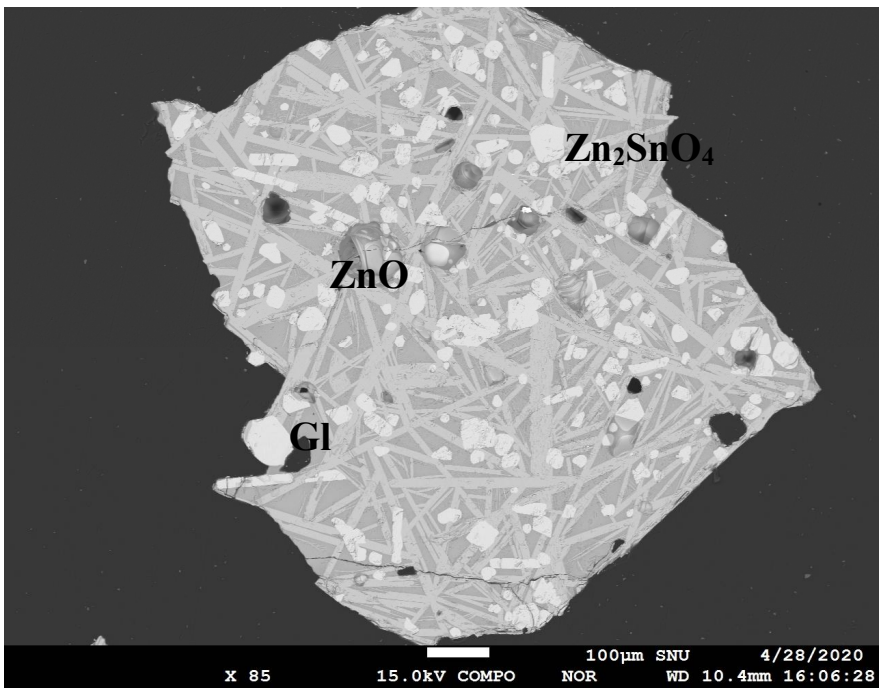

b)

Figure 4.2. Microstructure (BSE Images) of the quenched samples. a) IV and b) V of Table 4.2. (Gl: Glass).

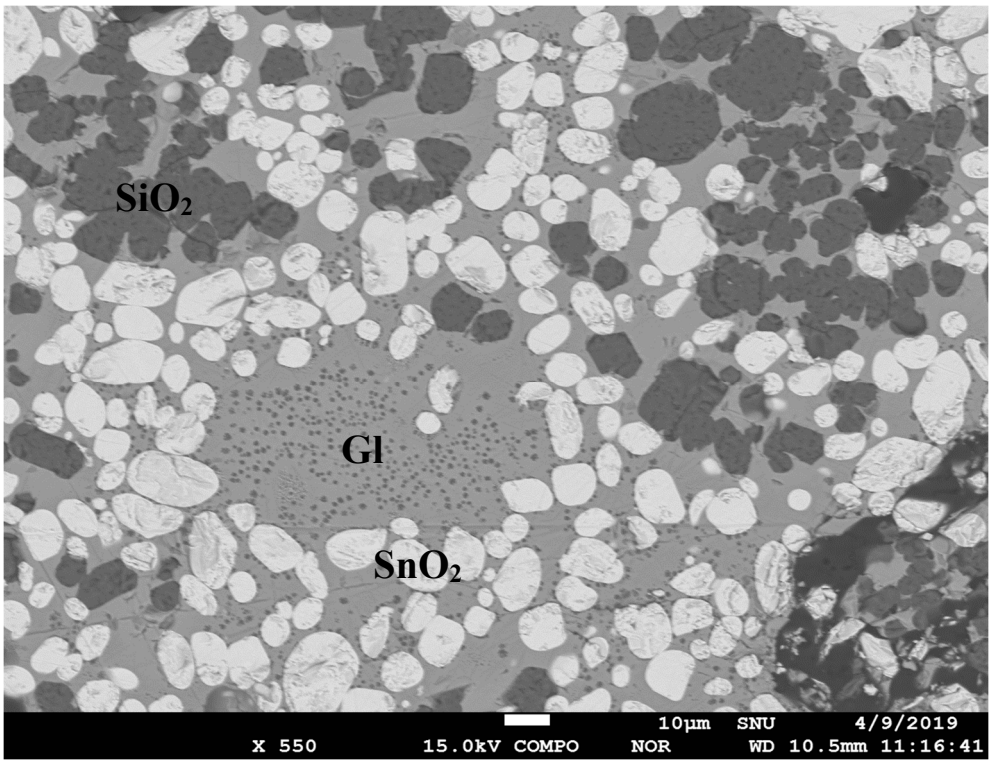
SiO2
Gl
SnO2
10µm SNU 4/9/2019
X 550 15.0kV COMPO NOR WD 10.5mm 11:16:41

a)

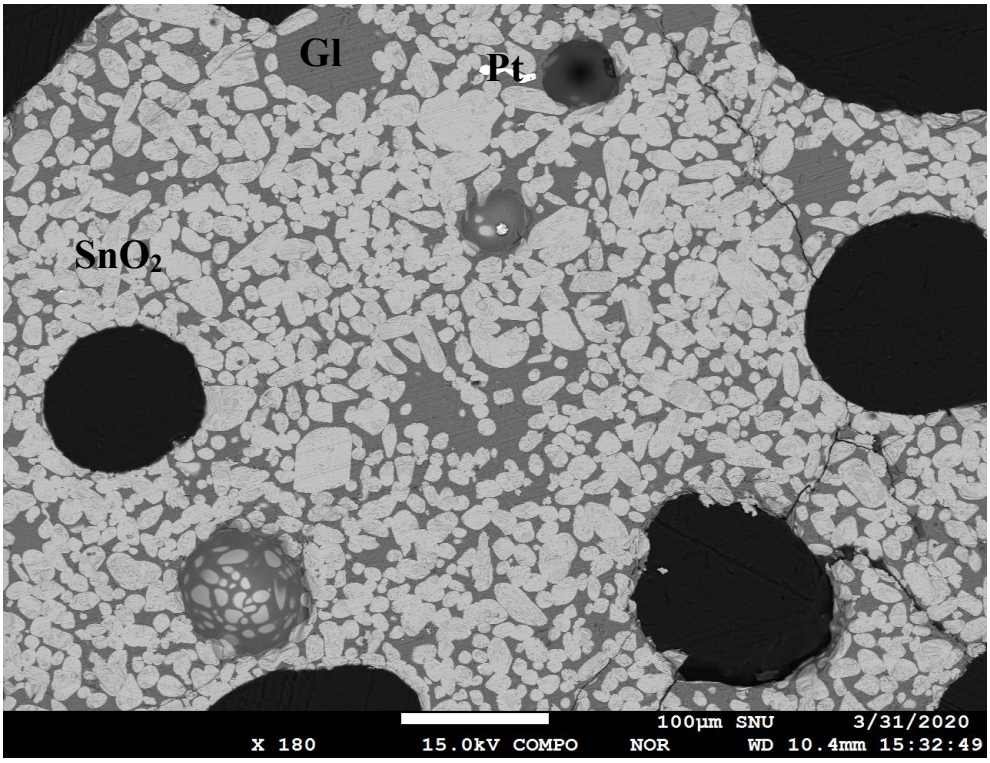
Gl
Pt
SnO2
100µm SNU 3/31/2020
X 180 15.0kV COMPO NOR WD 10.4mm 15:32:49

b)

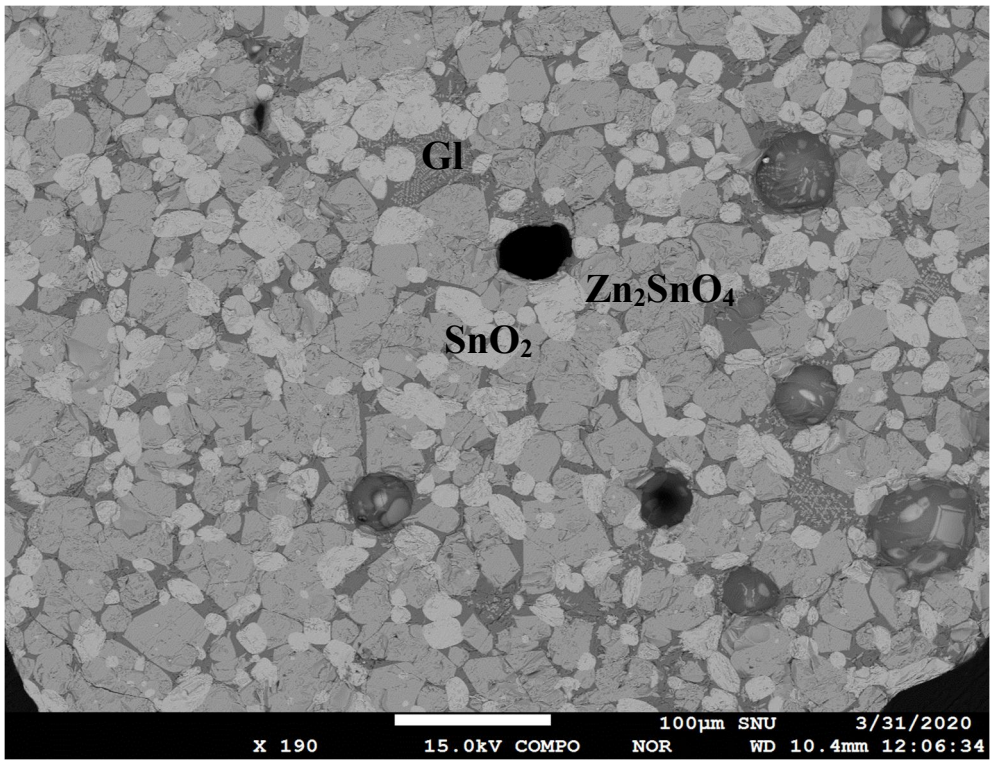
Gl
Zn_2SnO_4
SnO_2
100μm SNU 3/31/2020
X 190 15.0kV COMPO NOR WD 10.4mm 12:06:34

c)

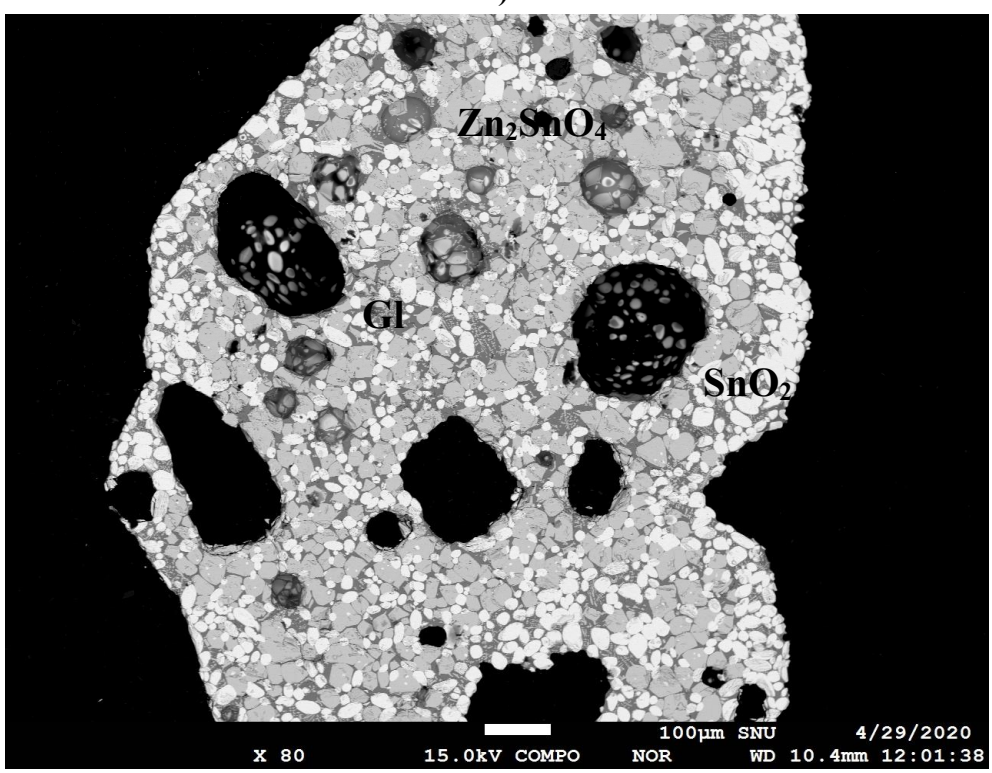
Zn_2SnO_4
Gl
SnO_2
100μm SNU 4/29/2020
X 80 15.0kV COMPO NOR WD 10.4mm 12:01:38

d)

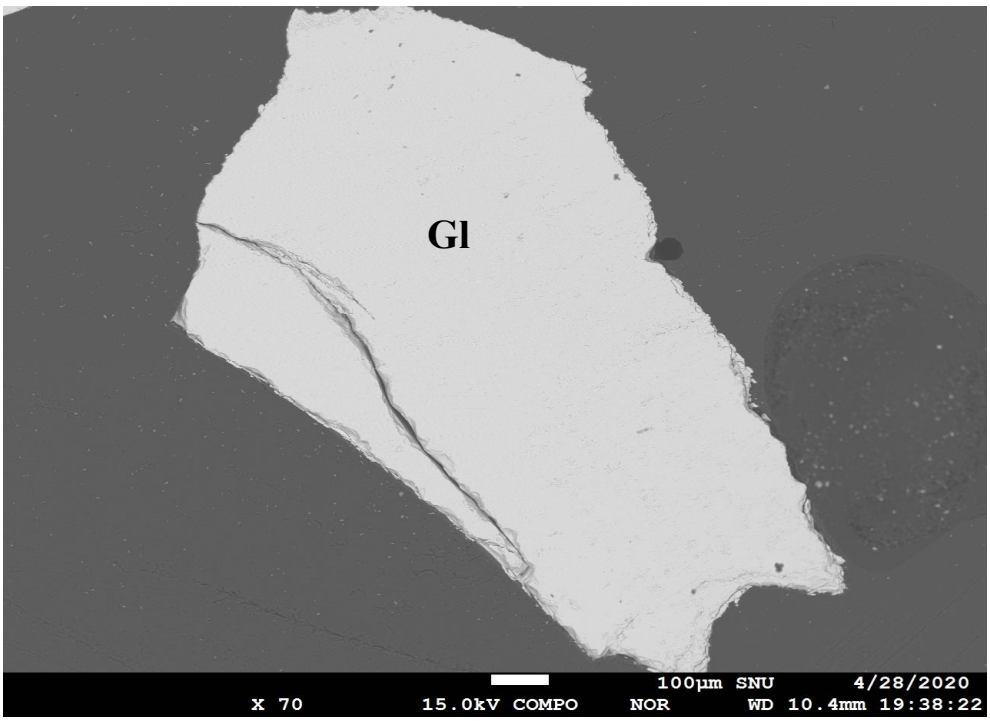

e)

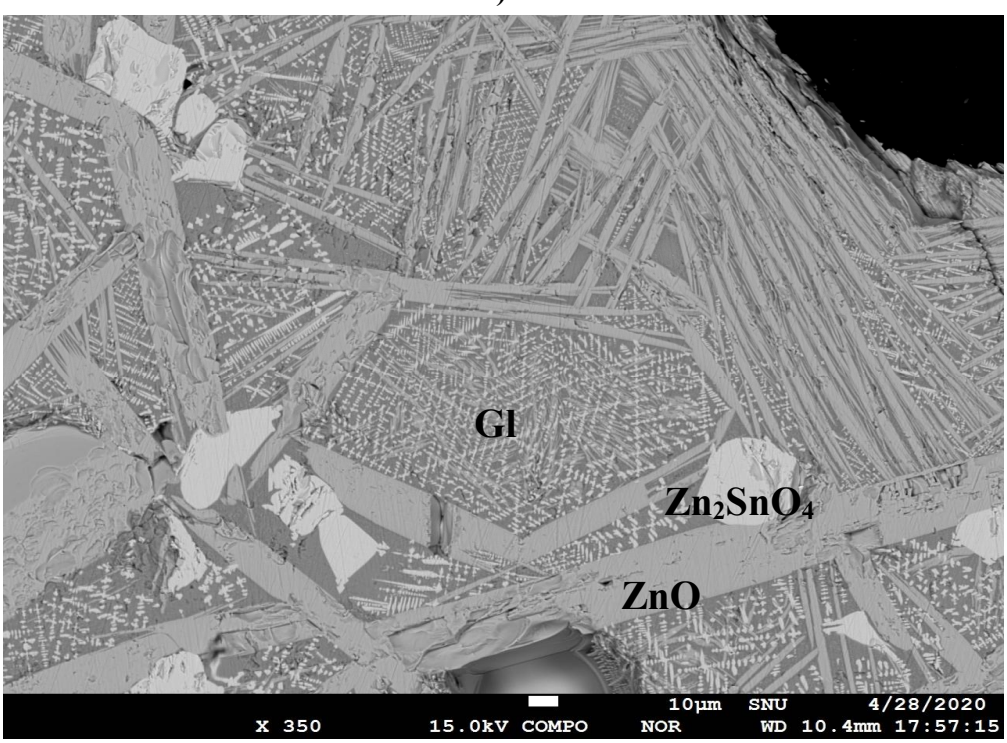

f)

Figure 4.3. Microstructure (BSE Images) of quenched samples. a) VI, b) VII, c) IX, d) X, e) XII and f) XIII of Table 4.2. (Gl: Glass).

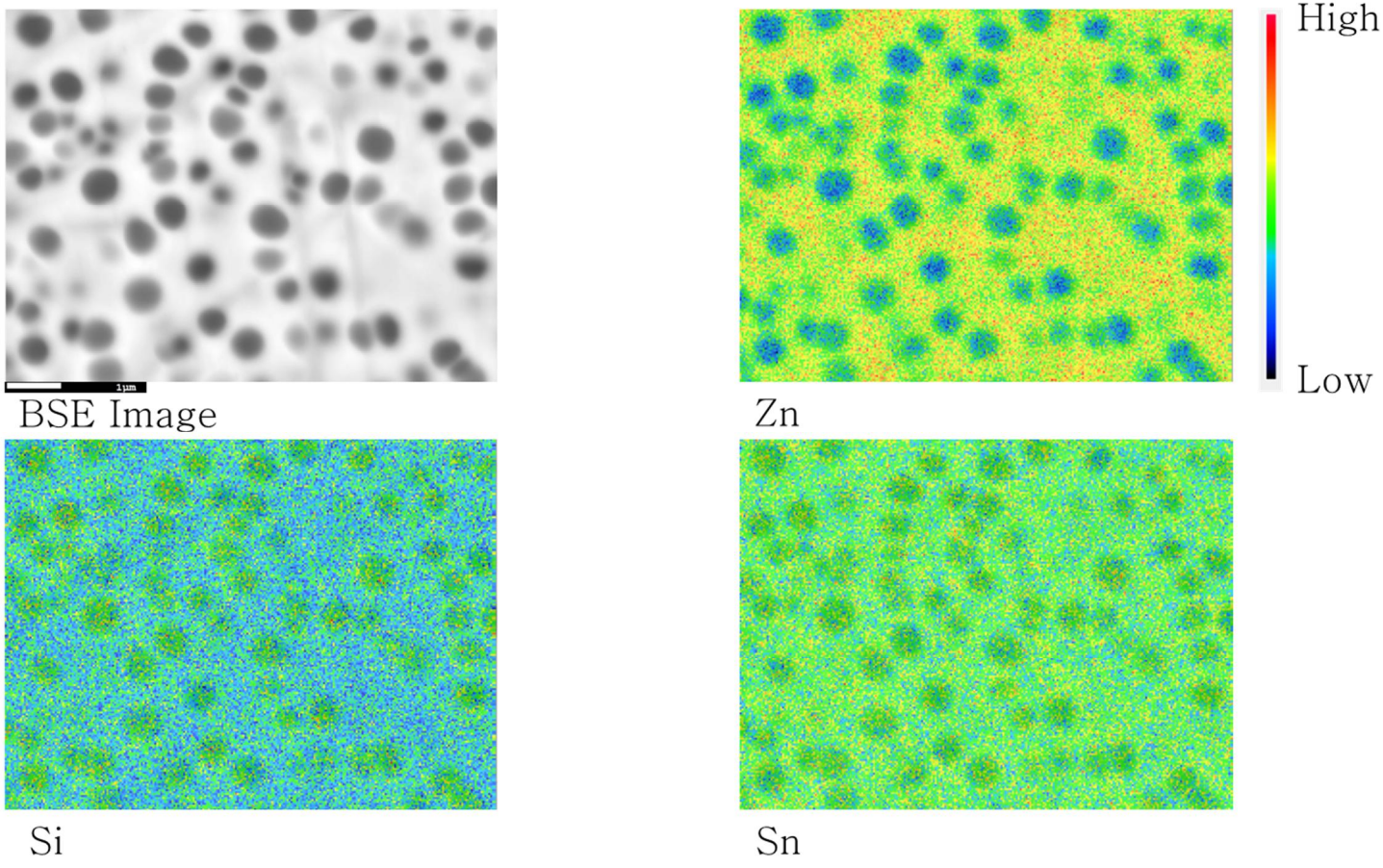

Figure 4.4. EPMA Mapping results of the precipitates in the sample VI of Table 4.2.

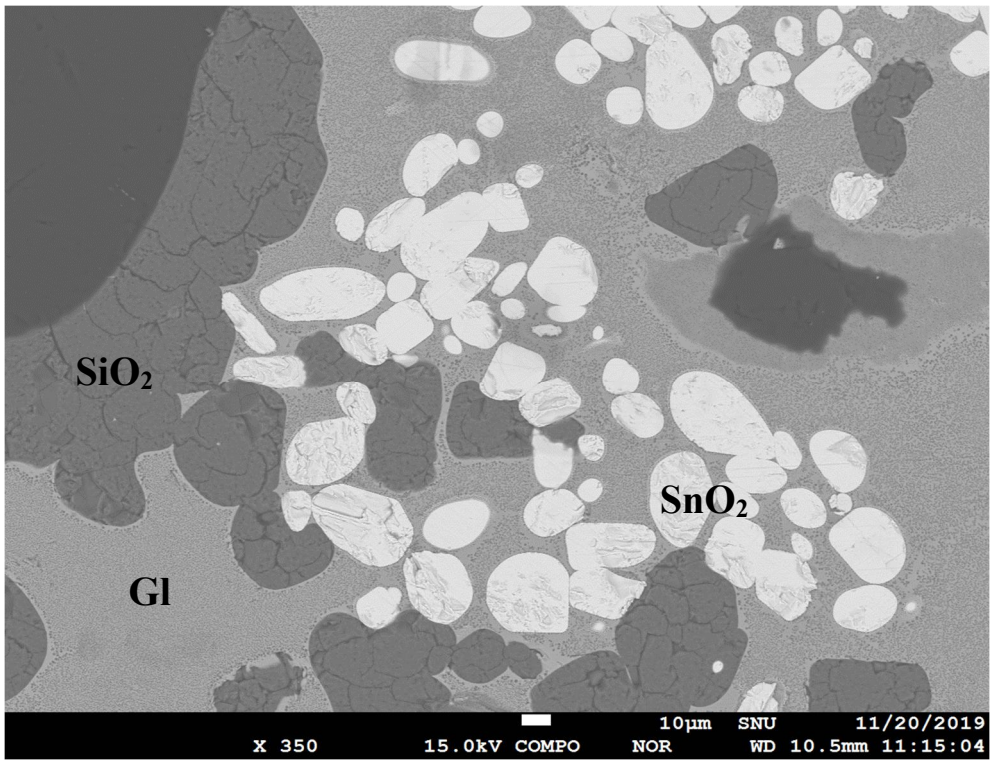
SiO2
SnO2
Gl
10μm SNU 11/20/2019
X 350 15.0kV COMPO NOR WD 10.5mm 11:15:04

a)

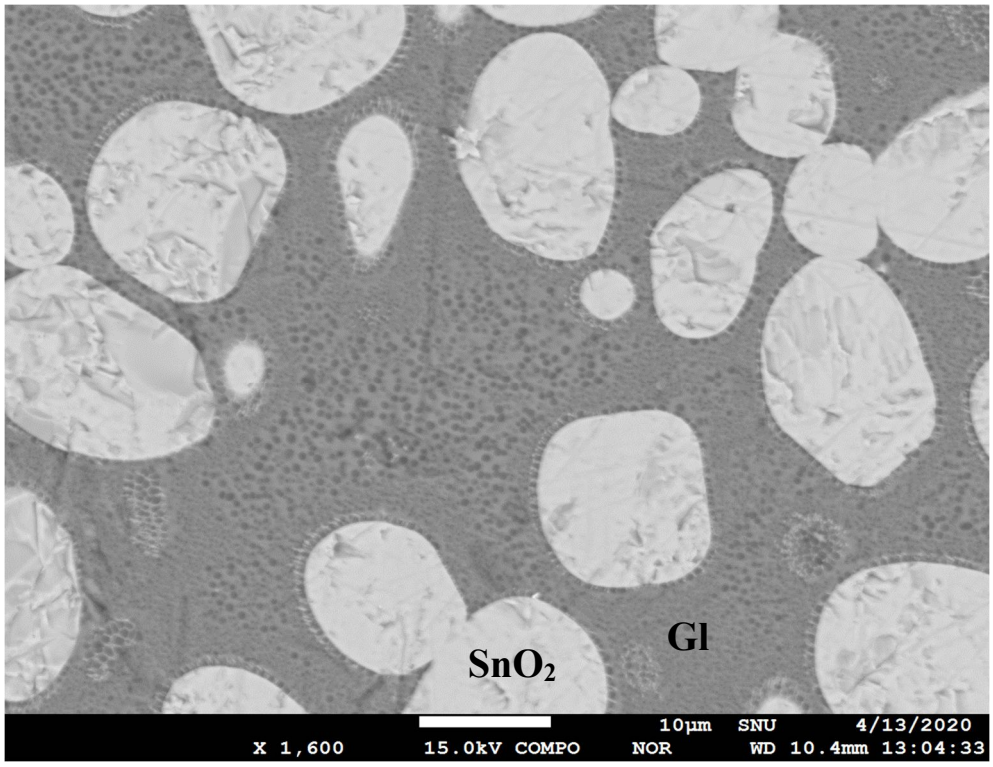
Gl
SnO2
10μm SNU 4/13/2020
X 1,600 15.0kV COMPO NOR WD 10.4mm 13:04:33

b)

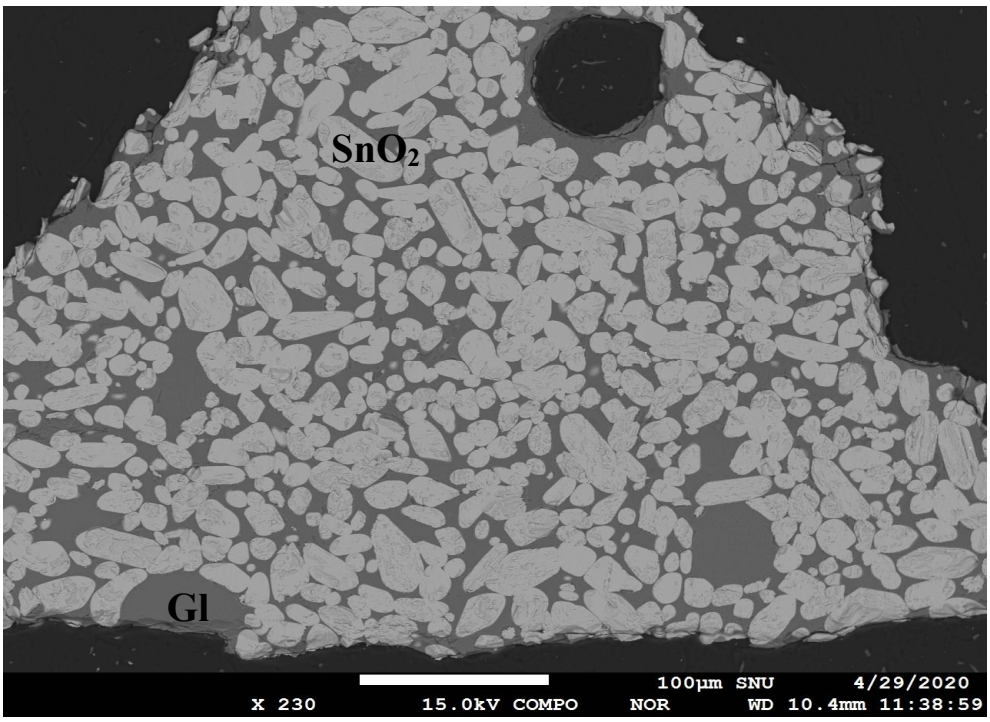

c)

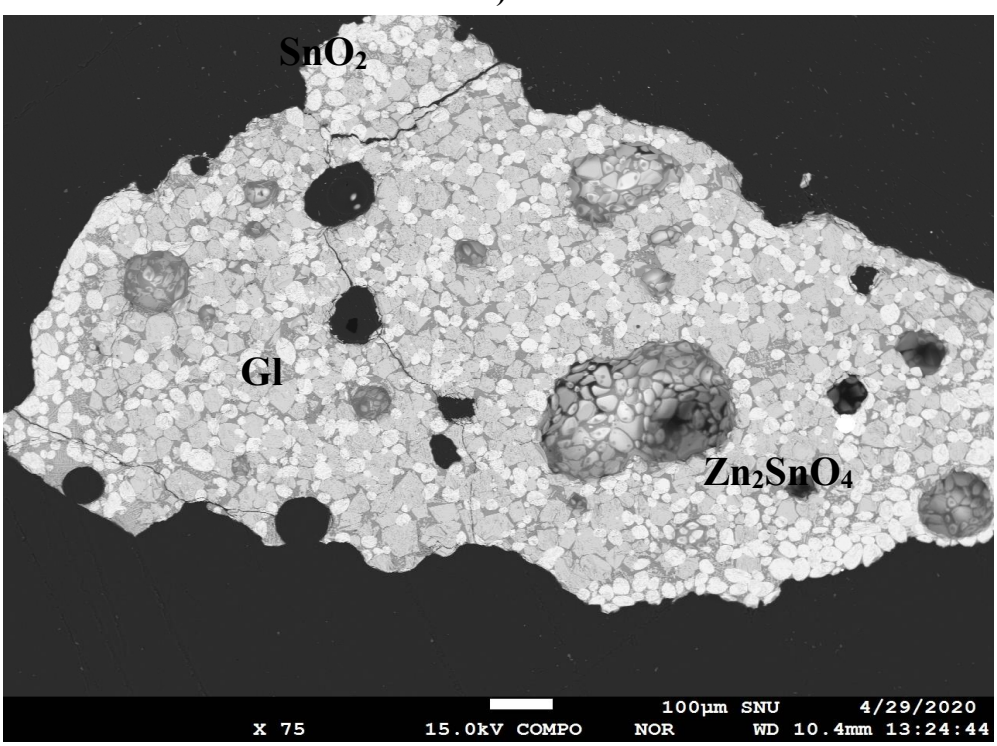

d)

Figure 4.5. Microstructure (BSE Images) of quenched samples. a) XIV, b) XVII, c) XV, and d) XVI of Table 4.2. (Gl: Glass).

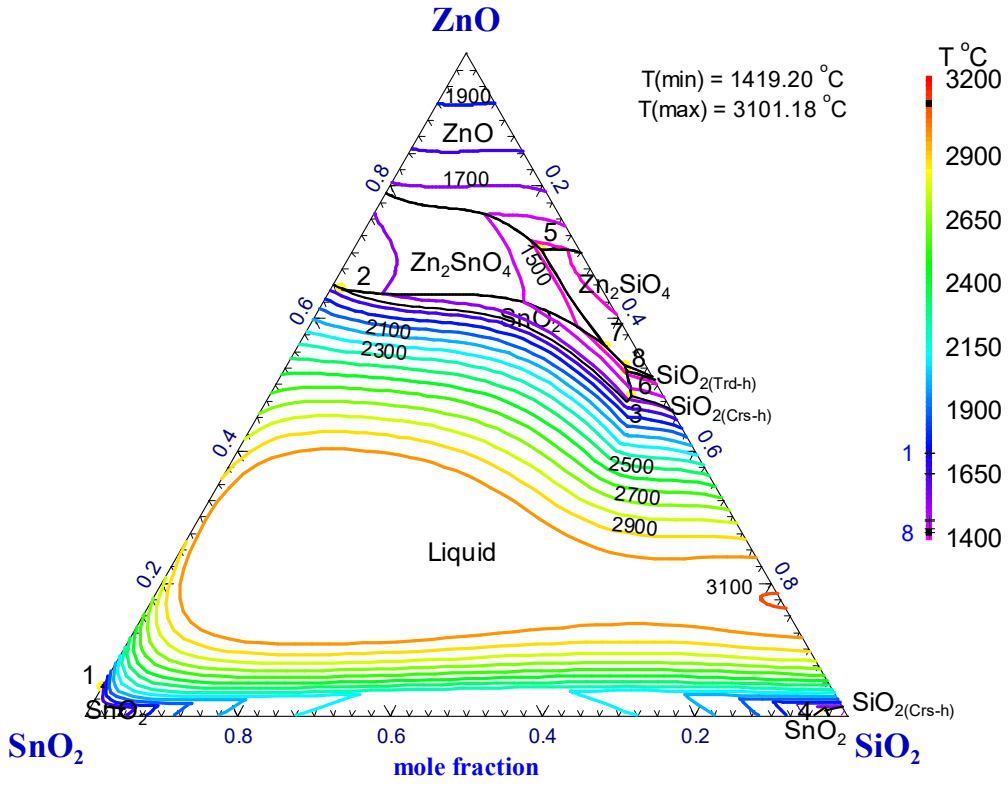

Figure 4.6. Predicted liquidus projection of the ZnO-SnO_2-SiO_2 system in the present study (See Table 4.3). Temperature in ºC.

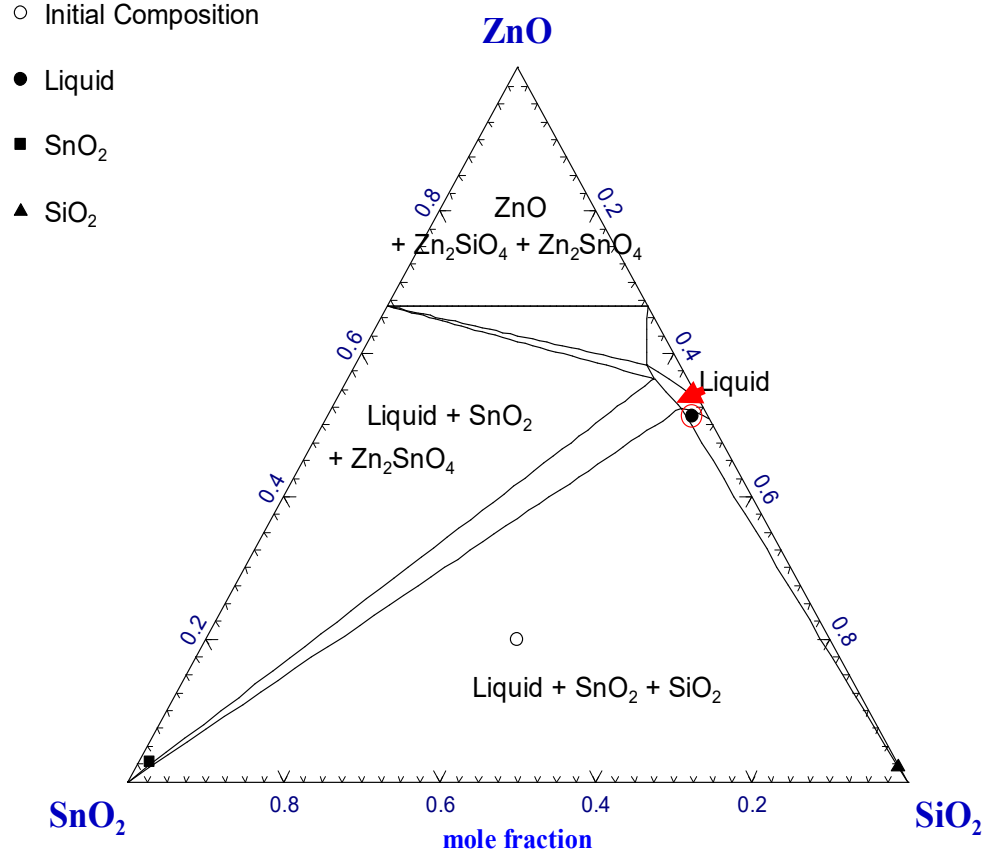
Initial Composition
Liquid
SnO2
SiO2
ZnO
ZnO
+ Zn2SiO4 + Zn2SnO4
Liquid
Liquid + SnO2
+ Zn2SnO4
Liquid + SnO2 + SiO2
0.8
0.6
0.4
0.2
SnO2
SiO2
mole fraction

a)

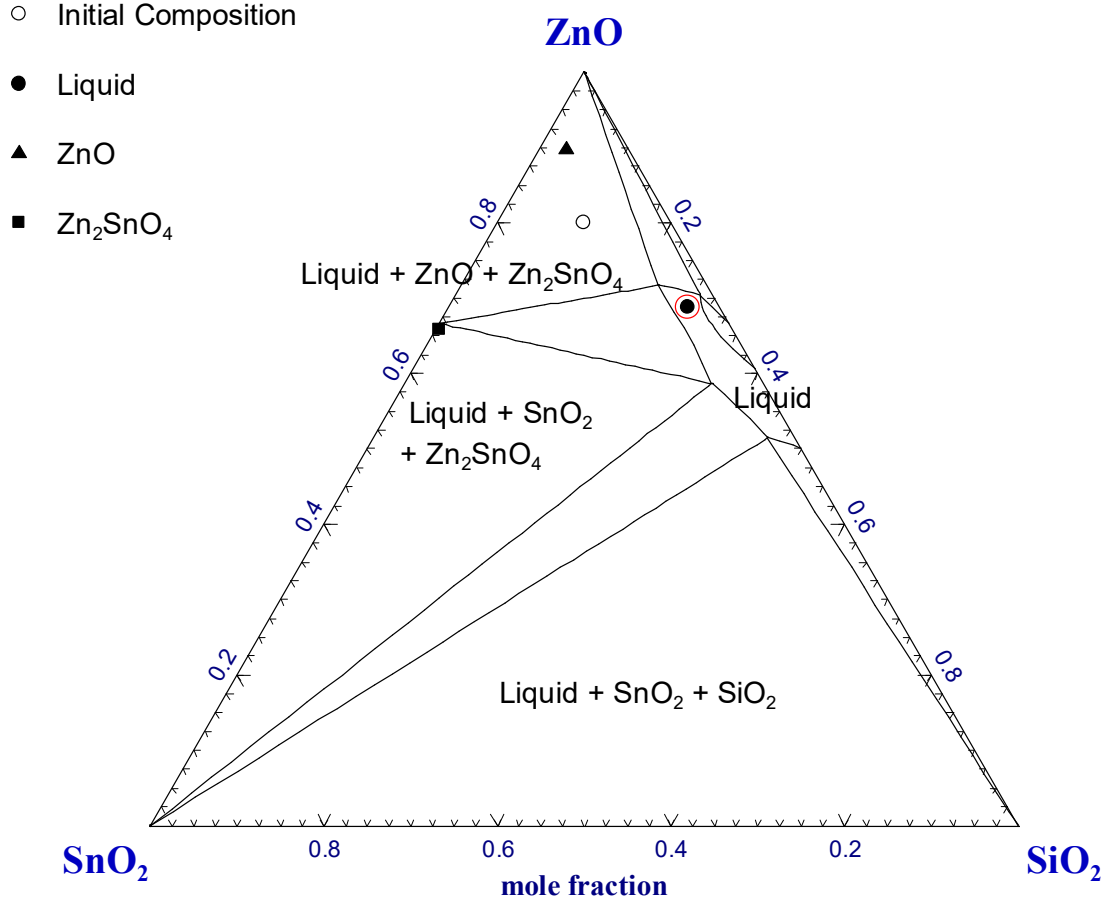
Initial Composition
Liquid
ZnO
Zn2SnO4
ZnO
Liquid + ZnO + Zn2SnO4
Liquid + SnO2
+ Zn2SnO4
Liquid
Liquid + SnO2 + SiO2
0.8
0.6
0.4
0.2
SnO2
SiO2
mole fraction

b)

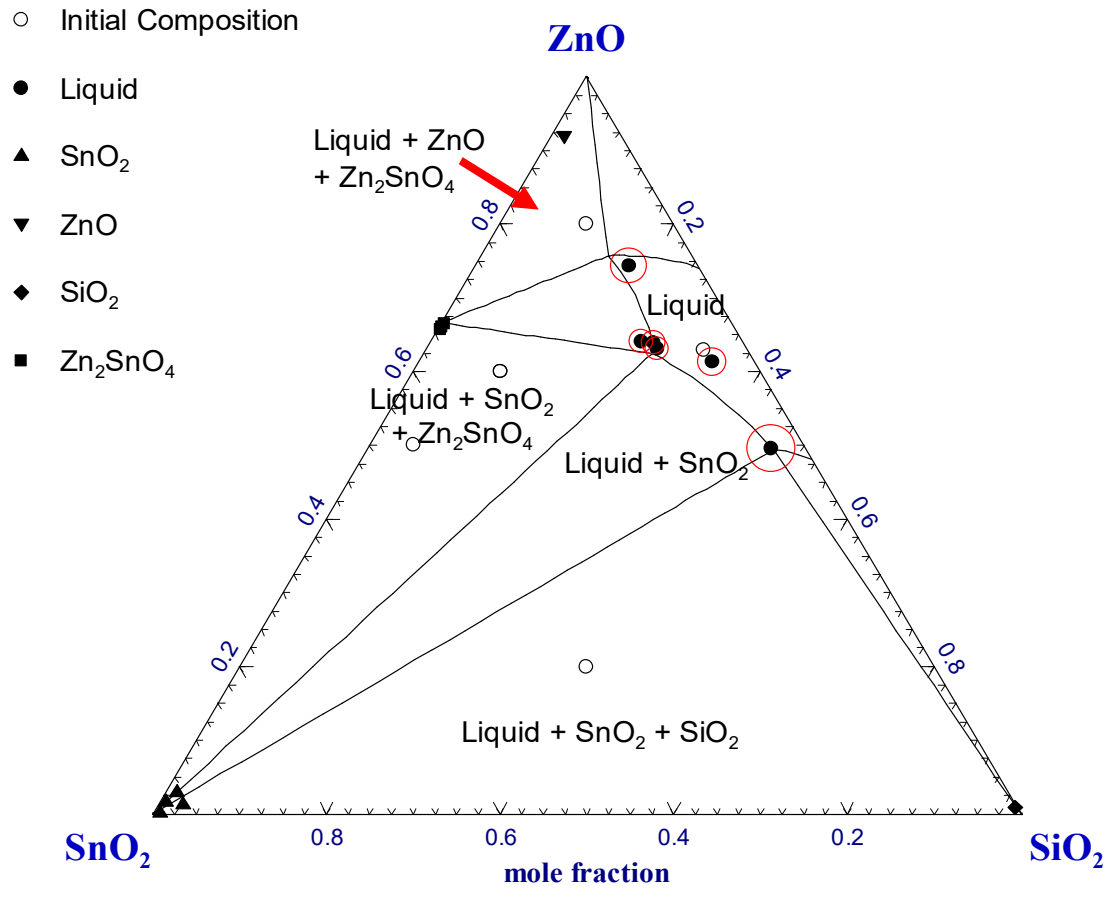
Initial Composition
Liquid
SnO2
ZnO
SiO2
Zn2SnO4
ZnO
Liquid + ZnO
+ Zn2SnO4
Liquid
Liquid + SnO2
+ Zn2SnO4
Liquid + SnO2
Liquid + SnO2 + SiO2
0.8
0.6
0.4
0.2
SnO2
SiO2
mole fraction

c)

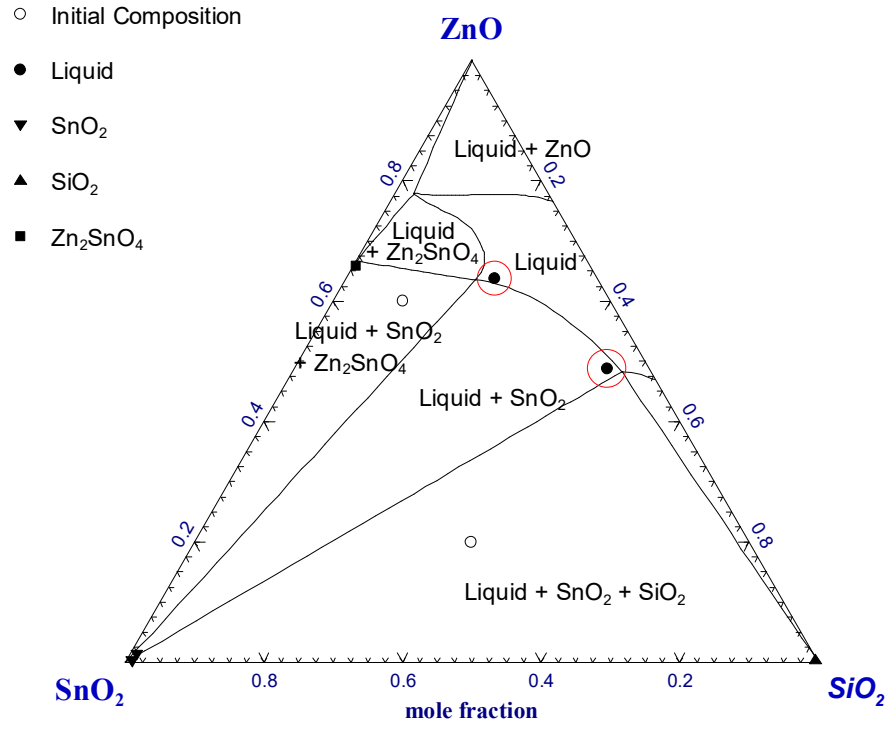

d)

Figure 4.7. Calculated isothermal phase diagram along with the present experimental results. a) 1450, b) 1500, c) 1600, and d) 1650°C. Filled small circle indicate the average composition of EPMA results, and large open circle presents the standard deviation of the analysis.

Table 4.1. Summary of the DTA experiments for the eutectic reactions in the ternary ZnO-SnO_2-SiO_2 system.

Sample	Starting Composition			Temperature (°C)	Rate (°C/min)	Transition (°C)
	X_{ZnO}	X_{SnO_2}	X_{SiO_2}			
I	0.2	0.4	0.4	25-1550	10	1424.6
II	0.8	0.1	0.1	25-1550	10	1464.8

Table 4.2. Summary of phase diagram experiments in the ternary ZnO-SnO_2-SiO_2 system (Gl: Glass).

Sample #	Initial Composition			Temperature (°C)	Duration (hr)	Phase Analyzed (XRD / EPMA)	Composition		
	ZnO	SnO2	SiO2				ZnO	SnO_2	SiO_2
I	0.2	0.4	0.4	1200	48	SiO_2			
						SnO_2			
						Zn_2SiO_4			
II	0.6	0.2	0.2	1200	48	SnO_2			
						Zn_2SiO_4			
						Zn_2SnO_4			
III	0.8	0.1	0.1	1200	48	ZnO			
						Zn_2SnO_4			
						Zn_2SiO_4			
IV	0.2	0.4	0.4	1450	1	Gl	0.512	0.021	0.467
						SiO_2	0.022	0.002	0.976
						SnO_2	0.028	0.958	0.013
V	0.8	0.1	0.1	1500	6	Gl	0.688	0.037	0.275
						ZnO	0.898	0.071	0.031
						Zn_2SnO_4	0.659	0.338	0.003
VI	0.2	0.4	0.4	1600	1	Gl	0.495	0.040	0.465

						SiO_2	0.009	0.002	0.989
						SnO_2	0.013	0.958	0.028
VII	0.4	0.35	0.25	1600	6	Gl	Unstable total and microstructure		
						SnO_2	0.010	0.982	0.008
VIII	0.4	0.35	0.25	1600	6	Gl	Unstable total and microstructure		
						SnO_2	0.001	0.992	0.008
IX	0.5	0.45	0.05	1600	6	Gl	0.639	0.104	0.257
						SnO_2	0.017	0.976	0.007
						Zn_2SnO_4	0.658	0.339	0.003
X	0.6	0.3	0.1	1600	6	Gl	0.641	0.117	0.243
						SnO_2	0.030	0.957	0.013
						Zn_2SnO_4	0.660	0.338	0.002
XI	0.6	0.3	0.1	1600	6	Gl	0.631	0.103	0.266
						SnO_2	0.002	0.991	0.008
						Zn_2SnO_4	0.657	0.340	0.003
XII	0.63	0.05	0.32	1600	3	Gl	0.614	0.048	0.338
XIII	0.8	0.1	0.1	1600	6	Gl	0.743	0.080	0.177
						ZnO	0.919	0.066	0.015
						Zn_2SnO_4	0.666	0.331	0.003

XIV	0.2	0.4	0.4	1650	20	Gl	0.488	0.061	0.451
						SiO_2	0.004	0.002	0.995
						SnO_2	0.014	0.976	0.010
XV	0.4	0.35	0.25	1650	3	Gl	Unstable total and microstructure		
						SnO_2	0.001	0.986	0.013
XVI	0.6	0.3	0.1	1650	3	Gl	0.637	0.149	0.215
						SnO_2	0.003	0.990	0.007
						Zn_2SnO_4	0.658	0.338	0.004
XVII	0.25	0.25	0.5	1675	3	Gl1	Unstable total and microstructure		
						Gl2			
						SnO_2	0.011	0.977	0.012

Table 4.3. Invariant reaction involving liquid in the ZnO-SiO2-SnO2 system predicted from the present study.

	Invariant reactions*	X(ZnO)	X(SnO_2)	X(SiO_2)	T (°C)
1	Liquid + SnO_2 + Zn_2SnO_4	0.0430	0.957	0.00048	1731.47
2	Liquid + SnO_2 + Zn_2SnO_4	0.645	0.341	0.01354	1731.47
3	Liquid + SnO_2 + SiO_2	0.483	0.0416	0.475	1650.83
4	Liquid + SnO_2 + SiO_2	0.0125	0.0226	0.965	1650.67
5	ZnO + Zn_2SnO_4 + Zn_2SiO_4	0.704	0.0492	0.247	1469.90
6	SnO_2 + $SiO_{2(Crs-h)}$ + $SiO_{2(Trd-h)}$	0.521	0.0297	0.449	1465.39
7	SnO_2 + Zn_2SnO_4 + Zn_2SiO_4	0.557	0.0381	0.405	1433.25
8	$SiO_{2(Trd-h)}$ + SnO_2 + Zn_2SiO_4	0.529	0.0277	0.443	1419.20

* Numbers indicating the invariant reactions in Figure 4.5.

Chapter 5. Conclusion

All the available thermodynamic properties and phase diagram data in the literature for binary ZnO-SnO_2 and SnO_2-SiO_2 system, and ternary ZnO-SnO_2-SiO_2 system were critically evaluated. Due to the lack of available experimental data, phase diagram experiments were conducted for the systems ZnO-SnO_2, SnO_2-SiO_2, and ZnO-SnO_2-SiO_2. Based on the new experimental data in the present study and available literature data, the binaries and ternary system were thermodynamically optimized using the CALPHAD methodology. In order to describe the Gibbs energy of the liquid solution, the Modified Quasichemical Model (MQM) was used, and all solid phases were treated as stoichiometric compounds. The MQM parameters were optimized to reproduce the phase diagram of the binary and ternary system accurately.

Based on the present experimental data and modeling results, the phase diagrams of the ZnO-SnO_2, SnO_2-SiO_2, and ZnO-SnO_2-SiO_2 were constructed for the first time. Using the thermodynamic models and optimized parameters, all the unknown thermodynamic properties within the system can be reasonably predicted, and any phase diagram within the system can be calculated within the experimental error limits. The present optimization results can be incorporated to the existing database in

FactSage^{TM} [1] and used for the thermodynamic calculations of multicomponent systems for better understating and designing industrial processes.

Although the present results are the best achievable at the current state, the following information would be helpful to complete understanding of the thermodynamics of the ZnO-SnO_2-SiO_2 system:

(1) Exact melting temperature of SnO2.

(2) Exact liquidus of ZnO-SnO2.

(3) Thermodynamic property data for liquid phase.

Appendix. Re-optimization of the Sn-O Phase Diagram and the Preliminary Studies on the Binary Phase Diagrams Containing SnO_2

Appendix-1. Introduction

Future work of this study includes the expansion of the SnO_2 containing database to a multi-component system containing ZnO and SnO_x (ZnO-SnO_2-SnO -SiO_2-CaO-Al_2O_3-…) for various practical industrial (glass making, pyrometallurgical) and research uses [8–10,25]. Thus, the phase diagram of Sn-O was re-optimized according to the new experimental and optimization results. Gibbs energies of some stoichiometric compounds in some of the binary systems (CaO-SnO_2, MgO-SnO_2, CoO-SnO_2) were optimized, and the literature reviews of some other systems (ZrO_2-SnO_2, MnO-SnO_2) were completed as well.

Methodology behind the redefinition of the melting point of SnO_2 is also presented. Literature review of previous efforts to measure the melting point of SnO_2 and the possible sources of error are explicated.

Appendix-2. Redefinition of the Melting Point of SnO_2

Figure appendix 1 shows a schematic diagram of the Gibbs energy to temperature diagram for solid, liquid, and gas phases of a single component system. At a given temperature, the phase with the lowest Gibbs energy is the most stable phase. The Gibbs energy of the liquid phase and the solid phase is identical at the melting point. Similarly, the Gibbs energy of the liquid and the gas phase is the same at the boiling point. For stoichiometric phases, all the Gibbs energy and phase transitions should be consistent. Thus, if the Gibbs energies of different states of a stoichiometric compound are known, the melting and the boiling point of one component system can be determined. If the melting or the boiling temperature of a stoichiometric substance is known, the Gibbs energy can be also estimated from the information.

The melting point of SnO_2 was redefined in this study. Coupled phase diagram experiments of various systems containing SnO_2 revealed that the previous reported melting point of SnO_2 (1625~1630^oC), may be erroneous. The new melting point of SnO_2 was estimated as 1750^oC.

Appendix-2.1. Literature Review

Multiple efforts were made to measure the melting point of SnO_2. Extensive review of the melting point of SnO_2 is provided by Yin [21]. Spandau and Kohlmeyer [26] estimated the melting point of SnO_2 as 2000^oC, but the

method for estimation was not given. The melting point provided by the two authors was used to optimize the phase diagrams of the Sn-O system. After, Barczak and Insely [27] estimated and modeled the phase diagram of SnO_2-Al_2O_3. The melting point of SnO_2 and the solidus temperature were measured by DTA analysis and was reconfirmed by multiple quenching experiments. The melting temperature of SnO_2 was measured as $1630\pm5^{o}C$. This agreed well with Ruff et al.'s study [28], who investigated the melting behavior of SnO_2 by heating SnO_2 inside a ZrO_2 crucible in N_2 atmosphere. Thus, the melting point of SnO_2 was previously optimized as $1625^{o}C$.

Appendix-2.2. The SnO_2-Al_2O_3 System

To check the accuracy of the melting point of SnO_2, and to validate Barczak and Insely's experimental data [27] for the SnO_2-Al_2O_3 system, differential thermal analysis (DTA) and coupled phase diagram experiment of SnO_2-Al_2O_3 system was conducted.

Appendix-2.2.1. Experimental Method

DTA and coupled phase diagram experiments for the starting composition of $0.5SnO_2$-$0.5Al_2O_3$ were conducted. The starting material was prepared by mixing SnO_2 and Al_2O_3 (Sigma Aldrich; purity 99.99%) in an agate mortar

with C_6H_{12}-cyclohexane liquid for 15 minutes. The sample was stored in cyclohexane to prevent any moisture or impurity pick-up. Before use, the samples were dried in vacuum oven at 75ºC. The samples were put in sealed Pt capsules for the DTA and quenching experiments at high temperature. The DTA, quenching experiments, and the phase characterizations were all completed in the same way outlined in Chapters 3 and 4.

Appendix-2.2.2. Results and Discussion

DTA was first run to check if any transitions were existent below 1550ºC. As expected, no transitions were existent below 1550ºC (Figure appendix 2). Thus, quenching experiments at 1600ºC and 1650ºC for 6 and 3hrs for the same initial composition was conducted. XRD phase and EPMA analysis of the two samples revealed that solid SnO_2 and solid Al_2O_3 phases existed (see Figure appendix 3 and Table appendix 1). Back scattered electron (BSE) images of the two samples did not show much differences as well. SnO_2 and Al_2O_3 agglomerated but did not form clear grains and grain boundaries. No mutual solubilities were detected.

Appendix-2.2.3. Redetermination of the Melting Temperature of SnO_2

Based on the experimental results for the SnO_2-Al_2O_3 system, it was evident that the melting point of SnO_2 should be at least higher than 1650°C. Thus, quenching experiments at 1650 and 1680°C for pure SnO_2 were designed. Pure SnO_2 powder was put in sealed Pt capsules and were annealed at 1650 and 1680°C for 1 hr. After, the samples were quenched in water. No signs of sintering could be found. XRD phase also showed clear crystal peaks of SnO_2 (see Figure appendix 4). From the quenching of pure SnO_2, experimental results from the SnO_2-Al_2O_3 system, and all the binary and ternary phase diagram data of the ZnO-SnO_2-SiO_2, the melting temperature of SnO_2 was determined to be at least higher than 1680°C.

The previous melting temperatures of SnO_2 (1625~1630°C) were defined from the consistent experimental data of Ruff et al. and Barczak and Insely [27,28]. There are some possible sources of error that would have hindered the accurate determination of the melting point of SnO_2. First, the vapor pressure of SnO_2 is very high [11,21,29]. It would have been impossible to create a closed environment to contain SnO_2. The DTA peak that both papers observed would therefore be from the sudden volatization of SnO_2 at the temperature, not the melting of SnO_2 in an open environment. In this work, to avoid the problem, we utilized thick platinum tube to make a closed environment (4 mm outer diameter and 0.5mm wall thickness). Even in the case, containing SnO_2 was a challenge. Moreover, Ruff et al. [28] used ZrO_2

crucible to contain SnO_2 in an N_2 atmosphere. ZrO_2 can create a solid solution with SnO_2, and this would have also hampered the melting point measurement of SnO_2 [11].

There are many thermodynamic property data regarding $SnO_{2(s)}$ phase. No thermodynamic property data for $SnO_{2(l)}$ exist. Thus, ΔH_{fusion} of the SnO_2 was estimated assuming ΔS_{fusion} of SnO_2 is the same as that of TiO_2. The entropy of fusion is of iso-prototype (structure) phase could be similar [21]. $\Delta H^{o}_{298.15K}$ was recalculated assuming the melting temperature of SnO_2 to be 1750°C. The values of each are as follows:

$$\Delta H^{o}_{298.15K} = -553.06 \text{kJ/mol}$$

$$\Delta S^{o}_{298.15K} = 40.52 \text{ J/mol K}$$

$$c_p = 92 \text{ J/mol K}$$

Appendix-2.2.4. Thermodynamic Modeling of the SnO_2-Al_2O_3 System

From the present experiment, it was confirmed that there is no intermediate compound between Al_2O_3 and SnO_2 and that the liquidus between Al_2O_3 and

SnO_2 should be higher than 1650°C.

To reproduce the present experimental results, the binary MQM parameter $\Delta g_{Al^{3+}-Sn^{4+}}$ was optimized.

$$\Delta g_{Sn^{4+}-\ Al^{3+}} = 30000\ \text{J/mol}$$

A simple eutectic system was assumed. The calculated phase diagram of the SnO_2-Al_2O_3 system from the present optimization is presented in Figure appendix 5 along with experimental data. According to the present optimization, the eutectic temperature is 1655.9°C.

Appendix-3. Re-optimization of the Sn-O Phase Diagram

Defining the Sn-O system is crucial because the definition of the system is the first step to creating a complete SnO_x containing database. The re-optimization of the Sn-O phase diagram was completed (see Figure appendix 6). All model parameters were taken from Yin's previous work [21]. Only the thermodynamic property of $SnO_{2(l)}$ was changed to the values in Appendix 2.2.3.

The iso-oxygen partial pressure trajectory in the liquid Sn oxide solution was

predicted in the newly defined phase diagram of the Sn-O system (Figure appendix 7). This prediction tells the ratio of Sn^{2+} and Sn^{4+} at a given temperature and oxygen partial pressure. Sn^{2+}/Sn^{4+} increases with the increasing temperature. No experiments to determine the distribution of Sn^{2+}/Sn^{4+} exists.

Appendix-4. Binary Systems Containing SnO_2

Future work of this project is to build a comprehensive database that contains ZnO and SnO_x (ZnO-SnO_2-SnO-SiO_2-CaO-MgO-Al_2O_3-…). To build the comprehensive database, binary phase diagrams containing SnO_2 needs to be defined or redefined. Gibbs energies of some of the compounds in the binary phase diagrams containing SnO_2 has been optimized and some of the experimental phase diagrams containing SnO_2 has been critically reviewed.

Appendix-4.1. CaO-SnO_2 System

No phase diagram study of the CaO-SnO_2 binary system has been reported. However, experimental work and predictions in the multi-component systems containing CaO and SnO_2 has been conducted. In 2011, Xu et al. [30] studied the phase diagram of CaO-SnO_2-SiO_2 system in air by the quenching method.

Experiments were conducted in Al_2O_3 crucibles and the samples were held at target temperature from 2 to 24 hr. After, the homogeneities of all phases were tested by EPMA. However, this experimental study was primarily limited to the CaO-SiO_2 rich side of the ternary phase diagram because obtaining equilibria in the SnO_2 rich slag due to its volatization and corrosivity is a challenge. Preliminary predictions of the phase diagram have been made by Yin [21], who modeled the multi-component CaO-SnO-SnO_2-SiO_2 system.

Two compounds exist within the CaO-SnO_2 system: $CaSnO_3$ and Ca_2SnO_4. Jacob et al. [31] found the thermodynamic properties of mono- and dicalcium stannate in the temperature range of 700-1150°C by electromotive force measurement. The Gibbs energies of $CaSnO_3$ and Ca_2SnO_4 were modeled accordingly (see Figure appendix 8a and b and Table appendix 2. c_p of the compounds were estimated by the Neumann-Kopp rule [32] which calculates the c_p standard entropy of a complex oxide as the sum of the c_p and the standard entropies of its constituent oxides:

$$c_p\ (\text{Complex oxide}) = \sum c_p(\text{Constituent Oxides})$$

$$S^o_{298}\ (\text{Complex Oxide}) = \sum S^o_{298}\ (\text{Constituent Oxides})$$

Appendix-4.2. MgO-SnO_2 System

No experimental study has been done to study the phase diagram of the MgO-SnO_2 system. One compound, Mg_2SnO_4, exists in the system. Mg_2SnO_4 bears a spinel structure. Gibbs energy of formation for Mg_2SnO_4 was found by electromotive force measurement by Jacob et al. and S. Raghavan [31,33]. Enthalpy of formation of Mg_2SnO_4 was found by Navrotsky et al. [34] in 1976 by the high temperature Calvet-type twin microcalorimeter. The Gibbs energy of Mg_2SnO_4 was modeled accordingly (see Figure appendix 8 c and Table appendix 2). Mg_2SnO_4 is an entropy stabilized compound which the heat of formation from its component oxides is positive. The high entropy of the compound is a result of cation mixing in the octahedral site of the spinel. Jacob et al. predicted that Mg_2SnO_4 would be unstable below 207 ± 25^oC [35]. The decomposition of the compound would be very slow due to kinetic factors at low temperatures.

Appendix-4.3. CoO-SnO_2 System

No phase diagram study of the CoO-SnO_2 system has been conducted, but CoO is well known to improve the sinterability of SnO_2 [11,34,36,37]. Co_2SnO_4, which also bears a spinel structure, is the only compound reported in the system. The enthalpy of formation of the compound has also been studied by Navrotsky et al. [34], the Gibbs energy of the compound was modeled accordingly (see Table appendix 2).

Appendix-4.4. $MnO\text{-}SnO_2$ System

The $MnO\text{-}SnO_2$ spinel is a candidate among the future Li-ion tin oxide spinel based batteries [38]. The existence of the spinel phase in the system within $Mn_2SnO_4\text{-}Mn_3O_4$ in air and argon atmosphere has been studies by Inagaki et al. [39] (see Figure appendix 9 a and b). The mixture of Mn_3O_4 and SnO_2 in was heated in platinum crucibles in argon and air atmospheres in the temperature ranges of 1050 and 1300°C. After heating the samples twice for 24hr, and then cooled down to room temperature at roughly 15°C/minute speed. The samples were characterized by XRD. In argon, single phase spinel of Mn_2SnO_4 was achieved only above 1300°C. In air, the spinel single phase was only detected in the limited region close to Mn_3O_4. No Sn^{4+} ion was incorporated into the spinel structure below 1050°C because the stability of Mn^{2+} is very low in air atmospheric condition.

Appendix-4.5. $SnO_2\text{-}ZrO_2$ System

The effect of various additives such as SnO_2 to zirconia-based ceramics has been extensively studied in the past. Kim et al. [40] studied the effect of tetravalent dopants in zirconia by Raman spectra and found about 3.5 mol% GeO_2, 21 mol% CeO_2, 16 mol% TiO_2, and 8 mol% SnO_2 incorporation in tetragonal zirconia. Dhage [41] et al. synthesized $Sn_{0.75}Zr_{0.25}O_2$ phase using

the sol-gel method and analyzed the synthesized product by XRD phase and TEM analysis. Gaillard-Allemand et al. [11] studied the SnO_2-ZrO_2 phase diagram in the temperature range of 1230 and 1750°C and found an existence of an immiscibility gap, resulting in the two solid solutions of $(Zr_{1-x}Sn_x)O_2$ and $(Sn_{1-y}Zr_y)O_2$ (see Figure appendix 9 c). The starting powders were obtained by mixing the target compositions of SnO_2 and ZrO_2 always with 0.5 mol% of CoO to assist in sintering. The samples were annealed at a target temperature and cooled by removing them from the furnace. The analyses of the samples were completed by utilizing XRD phase analysis and EPMA.

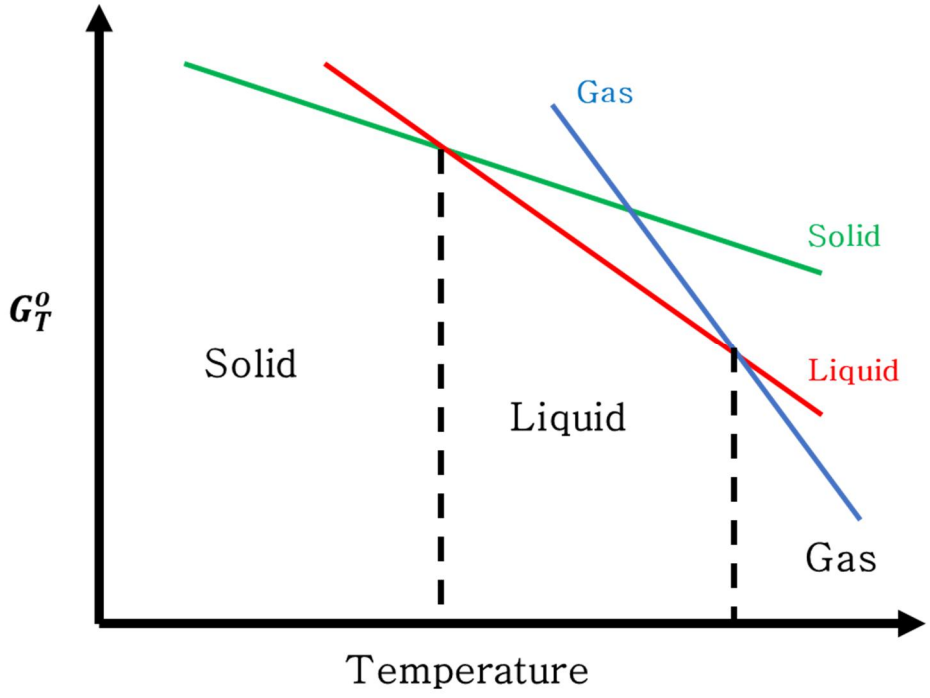

Figure appendix 1. Melting and boiling temperature.

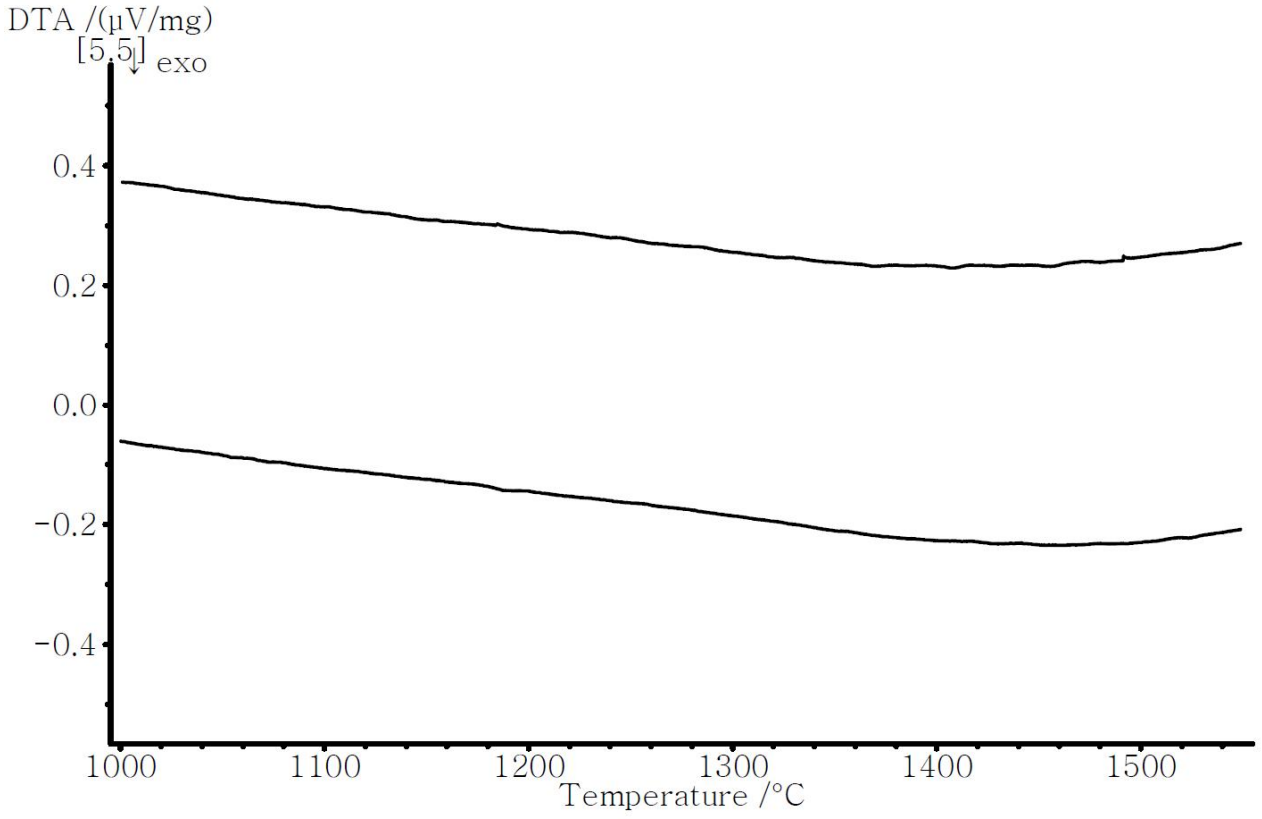

Figure appendix 2. Results of DTA for $X_{SnO_2} = 0.5$ sample in the binary SnO_2-Al_2O_3 system.

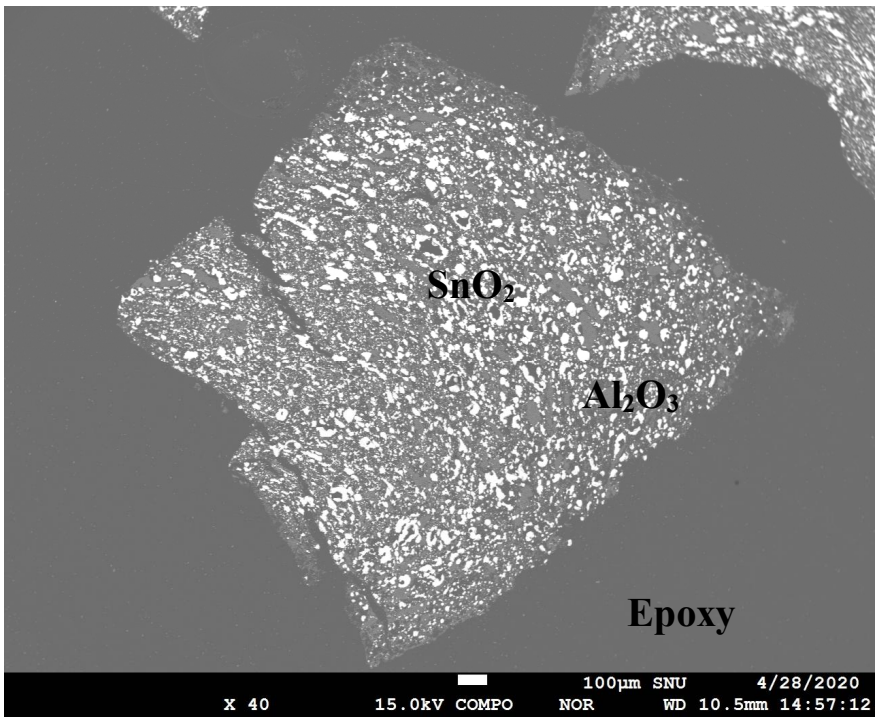

a)

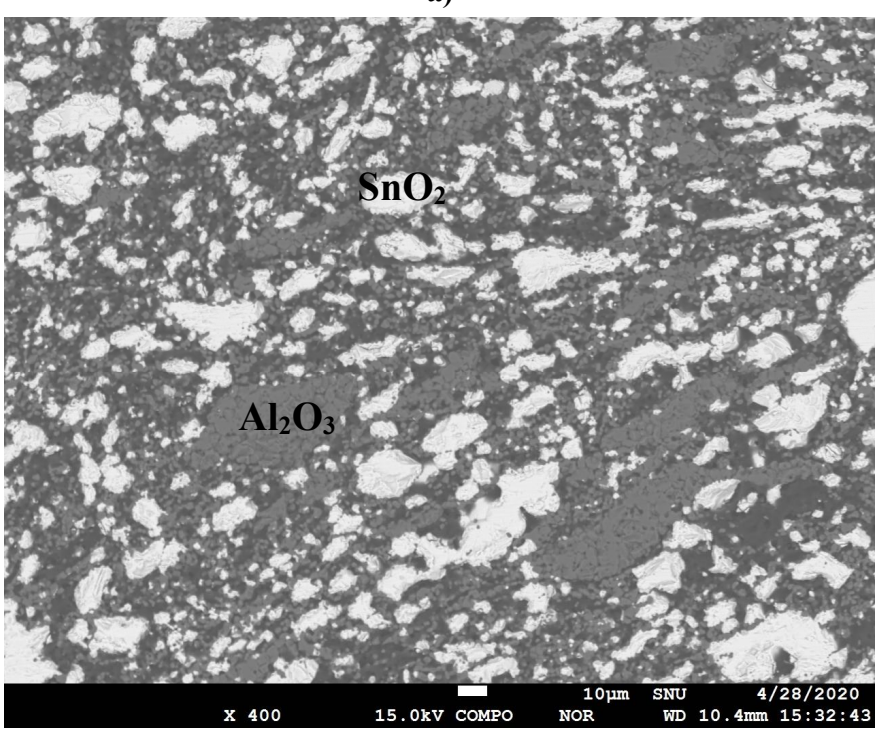

b)

Figure appendix 3. Microstructure (BSE Images) of quenched samples a) I and b) II of Table appendix 2.

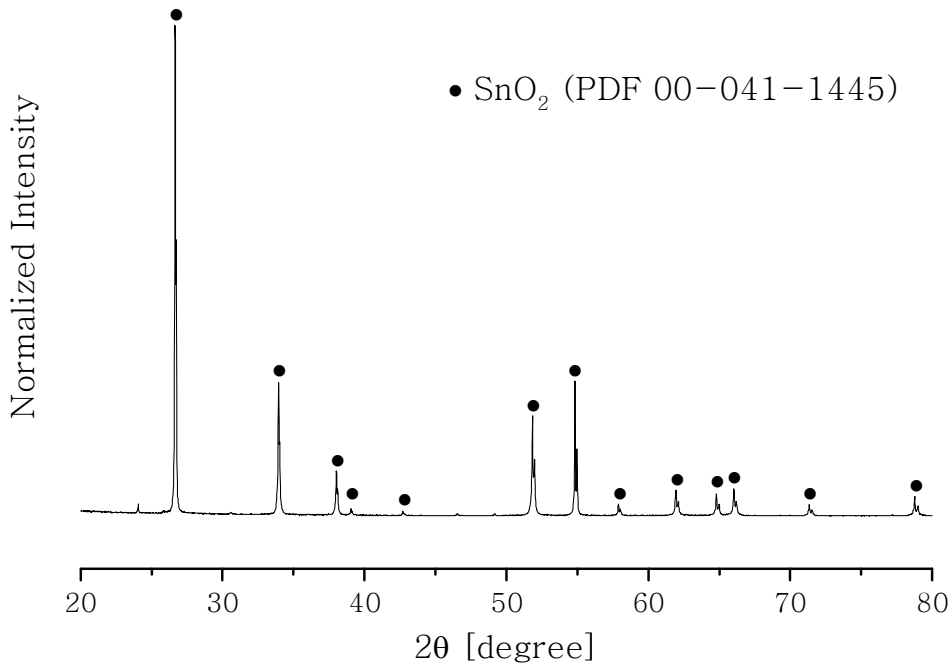

Figure appendix 4. XRD phase analysis of pure SnO_2 after equilibration at 1680ºC for 1hr.

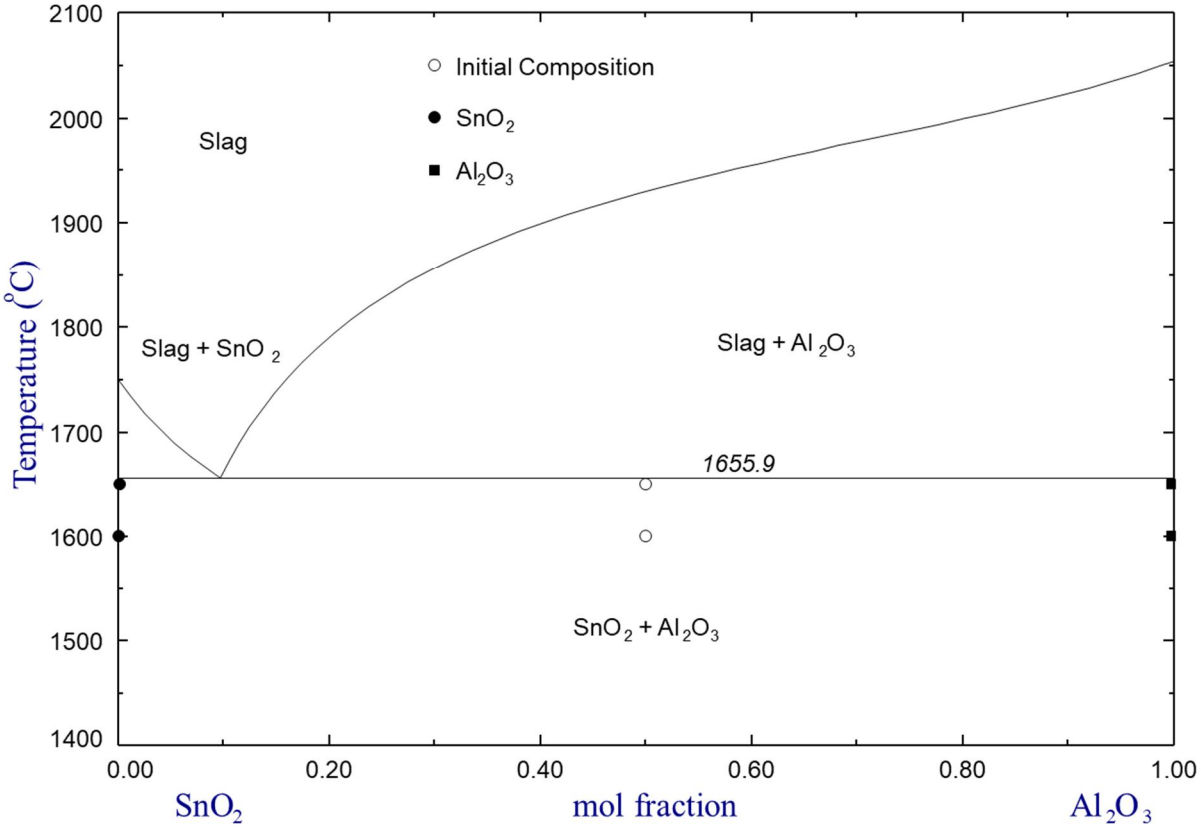

Figure appendix 5. The optimized phase diagram of the SnO_2-Al_2O_3 system along with present experimental data.

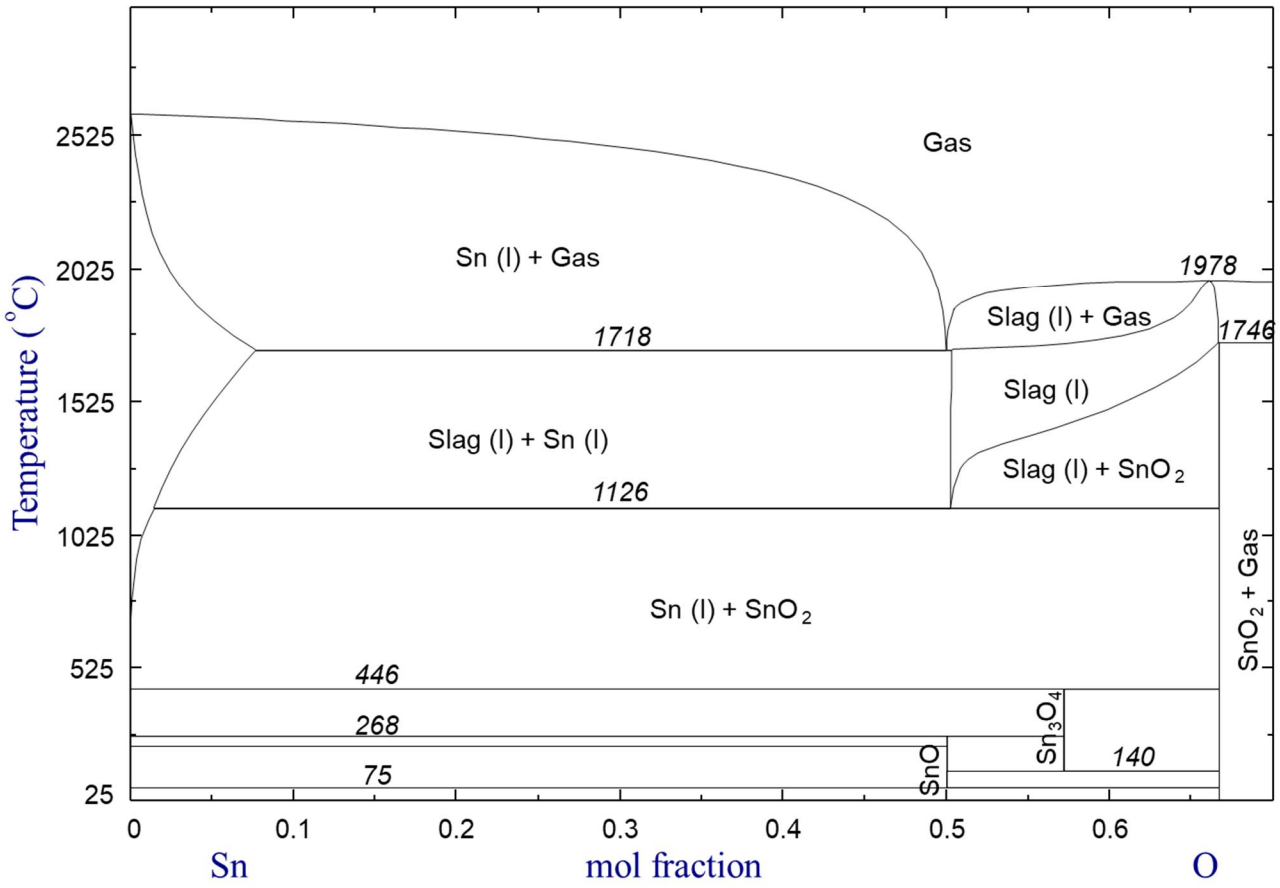

Figure appendix 6. The optimized phase diagram of the Sn-O system.

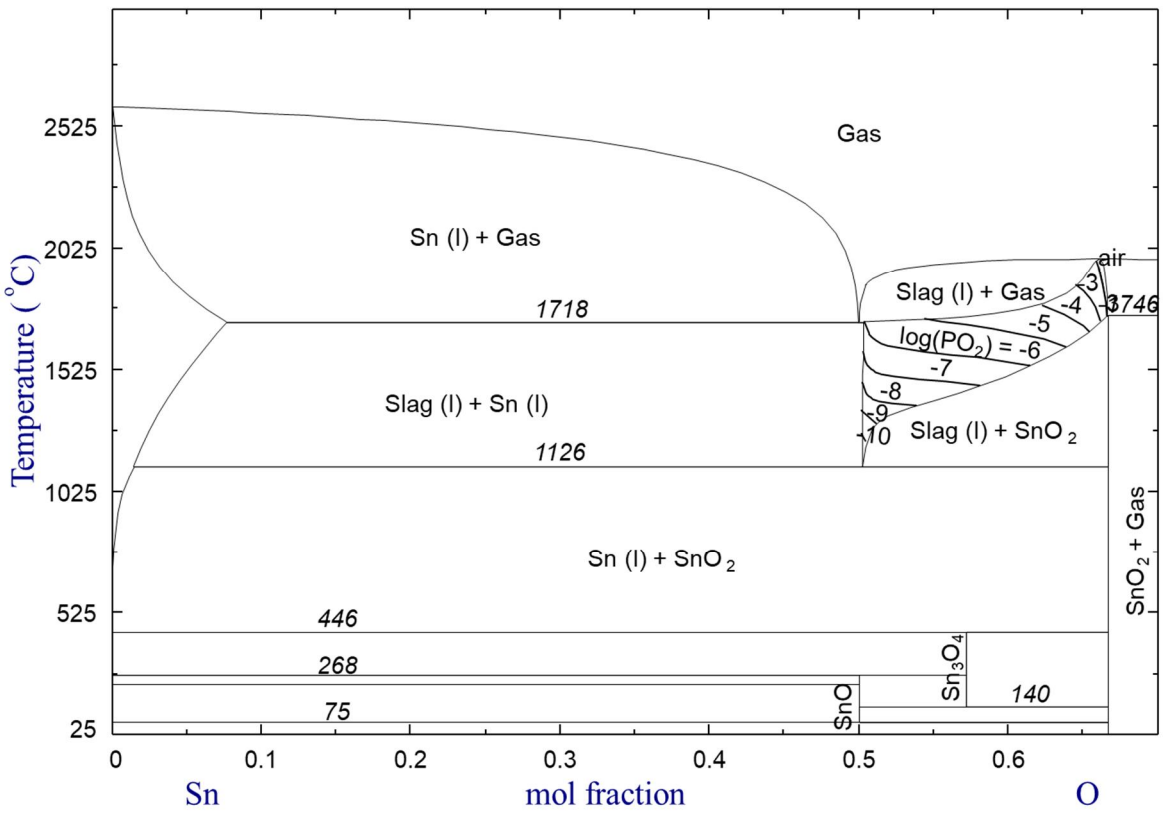

Figure appendix 7. Calculated iso-PO_2 (atm) contours in the liquid SnO-SnO_2 solution from the Sn-O system.

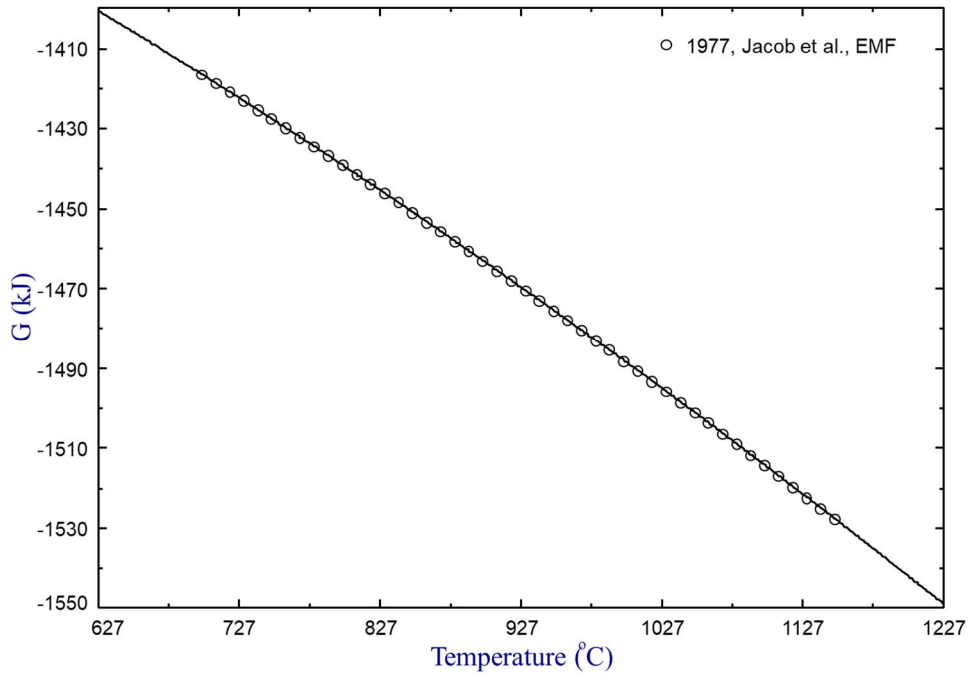
1977, Jacob et al., EMF
G (kJ)
-1410
-1430
-1450
-1470
-1490
-1510
-1530
-1550
627
727
827
927
1027
1127
1227
Temperature (°C)

a)

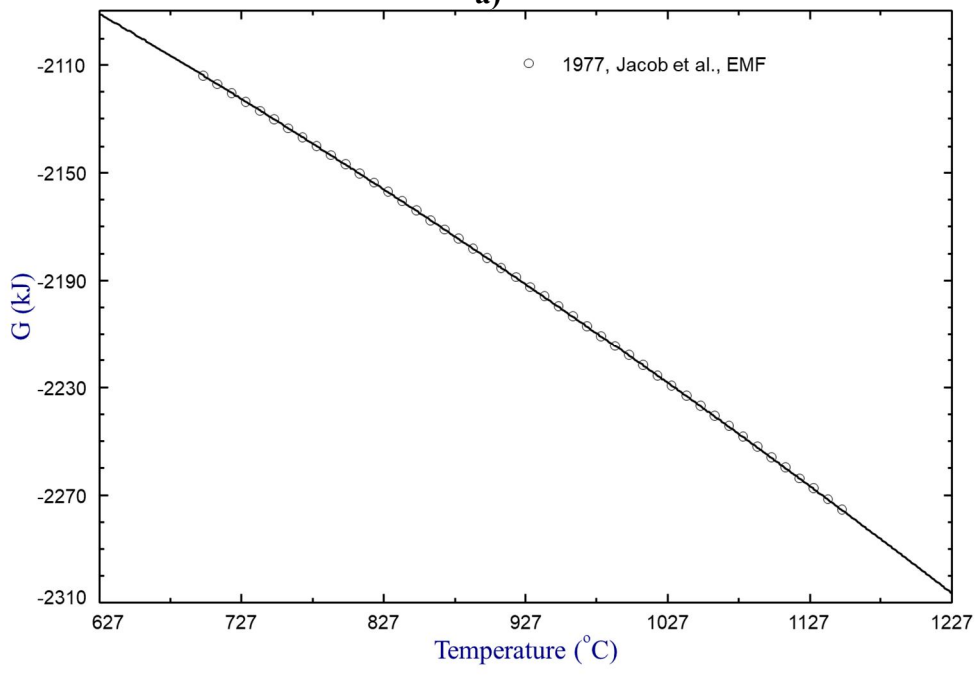
1977, Jacob et al., EMF
G (kJ)
-2110
-2150
-2190
-2230
-2270
-2310
627
727
827
927
1027
1127
1227
Temperature (°C)

b)

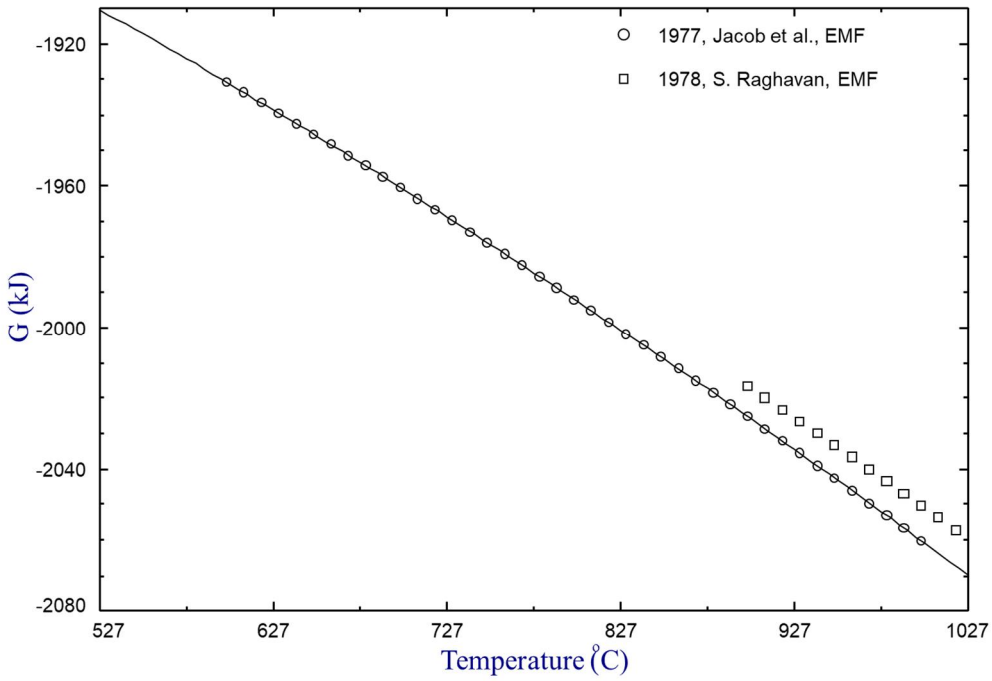

c)

Figure appendix 8. The optimized Gibbs energies of a) $CaSnO_3$ and b) Ca_2SnO_4 c) Mg_2SnO_4 along with experimental data.

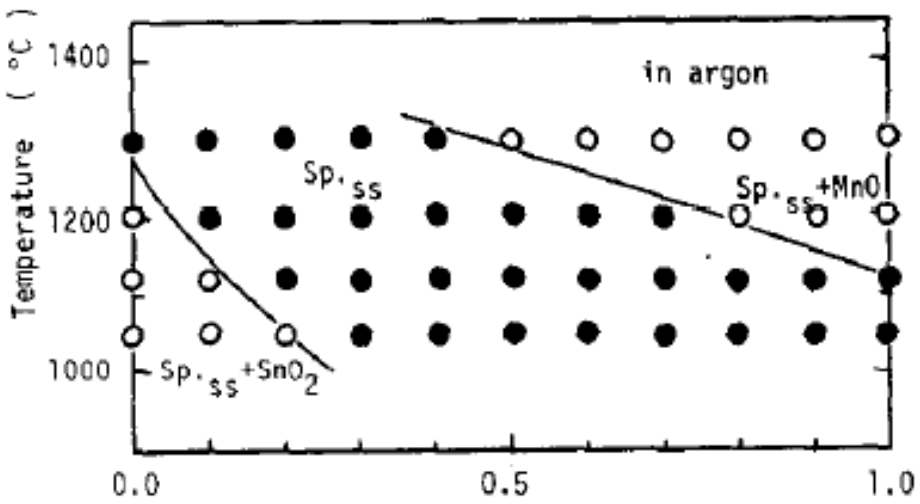
Temperature (°C)
1400
1200
1000
in argon
Sp.ss
Sp.ss+MnO
Sp.ss+SnO2
0.0
0.5
1.0

a)

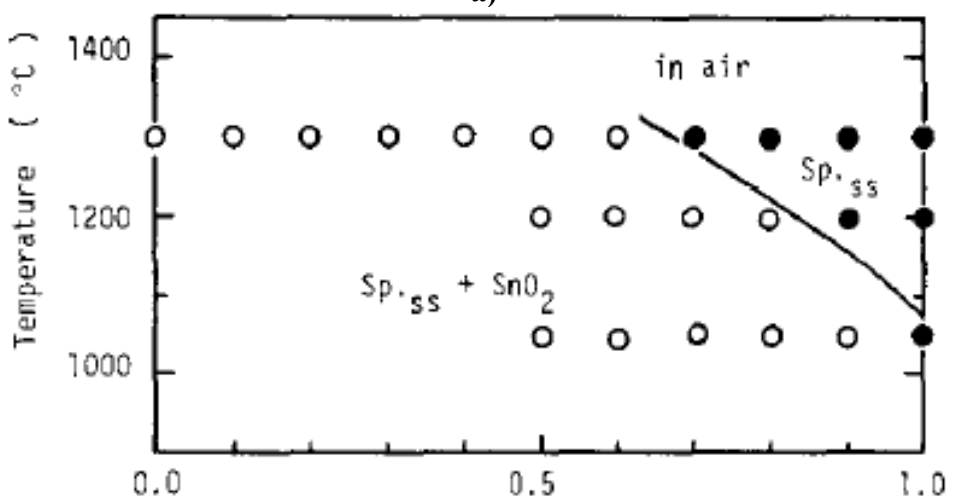
Temperature (°C)
1400
1200
1000
in air
Sp.ss
Sp.ss + SnO2
0.0
0.5
1.0

b)

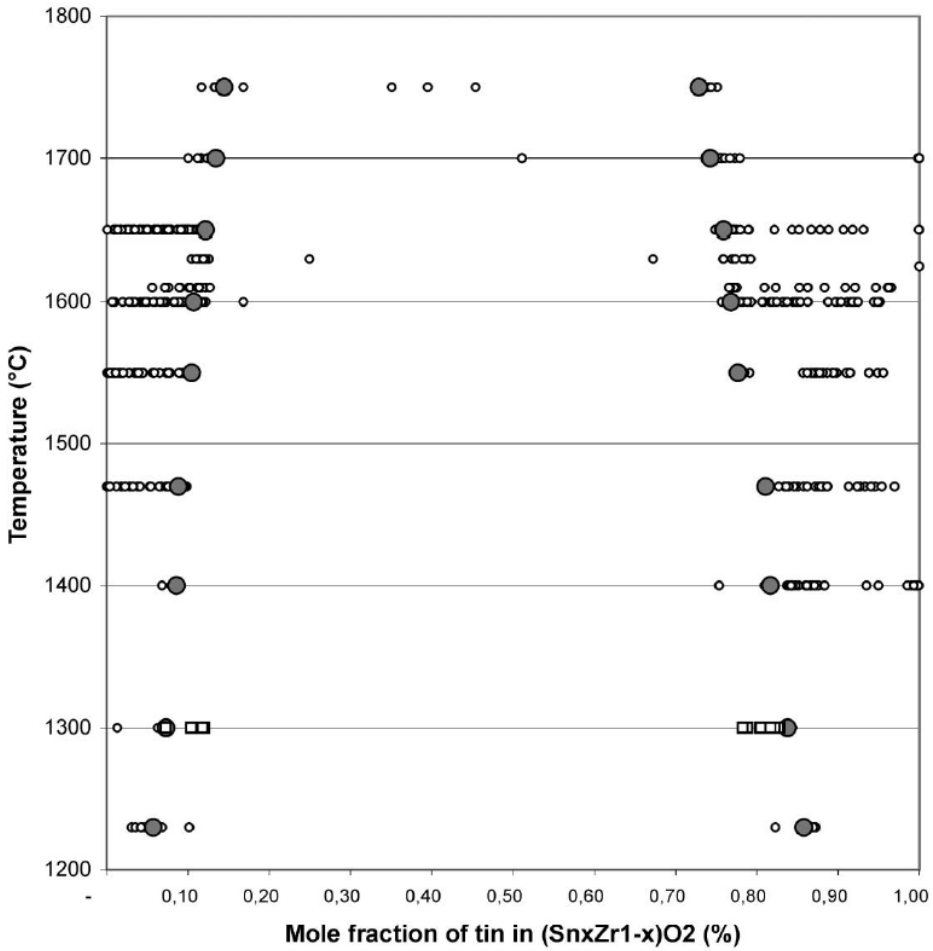

c)

Figure appendix 9. Equilibration results of the a) Mn_2SnO_4-Mn_3O_4 in argon condition b) Mn_2SnO_4-Mn_3O_4 in air condition c) SnO_2-ZrO_2 [11,39].

Table appendix 1. Summary of the equilibration experiments for the binary SnO_2-Al_2O_3 system.

Sample	Starting Composition (mol fr. SnO_2)	Temperature (°C)	Duration (hr)	Phases	EPMA Analysis	
					SnO_2 (mol fr.)	Al_2O_3 (mol fr.)
I	0.50	1600	6	$SnO_{2(s)}$	0.999	0.000908
				$Al_2O_{3(s)}$	0.00250	0.998
II	0.50	1650	3	$SnO_{2(s)}$	0.997	0.00280
				$Al_2O_{3(s)}$	0.00154	0.998

Table appendix 2. Summary of thermodynamic properties of the stoichiometric phases in the $CaO\text{-}SnO_2$, $MgO\text{-}SnO_2$, $CoO\text{-}SnO_2$ systems.

Phase	$\Delta H^{o}_{298.15}$ (kJ/mol)	$S^{o}_{298.15}$ (J/mol K)	C_p (J/mol K)	Reference
$CaSnO_3$	-1286.0000	78.0	$134.8322 + 0.007362T - 3371012.9825T^{-2} + 7.69E-10T^{2} - 133.9040T^{-0.5} + 102978787.8640T^{-3}$ $(25-1630°C)$ $148.2311 - 1147145.9825T^{-2} - 133.9040T^{-0.5} + 102978787.8640T^{-3}$ $(1630-2572°C)$ 152.1999 $(2572-3227°C)$	[31], This Work
Ca_2SnO_4	-1918.5000	121.5	$193.6233 + 0.007362T - 4818158.9650T^{-2} + 7.69E-10T^{2} - 267.8080T^{-0.5} + 205957575.7280T^{-3}$ $(25-1630°C)$ $207.0222 - 2294291.9650T^{-2} - 267.8080T^{-0.5} + 205957575.72800T^{-3}$ $(1630-2572°C)$ 214.9560 $(2572-3227°C)$	[31], This Work
Mg_2SnO_4	-1774.6887	115.3	$198.2603 + 0.007362T - 3466175.0082T^{-2} + 7.69E-10T^{2} - 592.3980T^{-0.5} + 11689224.0544T^{-3}$ $(25-1630°C)$ $211.6592 - 1242308.0082T^{-2} - 592.3980T^{-0.5} + 11689224.0544T^{-3}$ $(1630-2825°C)$	[33–35], This Work

Co_2SnO_4	-1062.7550	155.0	$223.3279\ \ (2825-3227℃)$ $186.807-0.005480T-2150267T^{-2}+1.4113E-5T^2\ \ (25-1327℃)$ $192.807-0.0136T-2676227T^{-2}-1.6941E-5T^2\ \ (1327-1630℃)$ $206.2060-0.02099T-452360T^{-2}-1.6941E-5T^2\ \ (1630-1830℃)$ $236.883\ \ (1830-3227℃)$	[34], This Work

Bibliography

[1] FactSage. www.FactSage.com. FactSage 7.3., (n.d.).

[2] N.A. Gribchenkova, A. V. Steblevsky, A.S. Alikhanyan, Vaporization thermodynamics of the ZnO-SnO_2 system, J. Chem. Thermodyn. 70 (2014) 203–206. https://doi.org/10.1016/j.jct.2013.11.010.

[3] A.D. Pelton, S.A. Degterov, G. Eriksson, C. Robelin, Y. Dessureault, The modified quasichemical model I - Binary solutions, Metall. Mater. Trans. B Process Metall. Mater. Process. Sci. 31 (2000) 651–659. https://doi.org/10.1007/s11663-000-0103-2.

[4] E. Ising, Beitrag zur theorie des ferromagnetismus, Zeitschrift Für Phys. A Hadron. Nucl. 31 (1925) 253–258.

[5] A.D. Pelton, A general “geometric” thermodynamic model for multicomponent solutions, Calphad Comput. Coupling Phase Diagrams Thermochem. 25 (2001) 319–328. https://doi.org/10.1016/S0364-5916(01)00052-9.

[6] P. Chartrand, A.D. Pelton, On the choice of “Geometric” thermodynamic models, J. Phase Equilibria. 21 (2000) 141–147. https://doi.org/10.1361/105497100770340192.

[7] M.C. Heuzey, A.D. Pelton, Critical evaluation and optimization of the thermodynamic properties of liquid tin solutions, Metall. Mater.

Trans. B Process Metall. Mater. Process. Sci. 27 (1996) 810–828. https://doi.org/10.1007/bf02915611.

[8] Q. Gong, Late Cretaceous aluminium A-type granites and its geological significance of Dasongpo Sn deposit, Tengchong, West Yunnan, Acta Petrol. Sin. 05 (2012) 1477–1492.

[9] A.G. Davies, M. Gielen, K.H. Pannell, E.R.T. Tiekink, Tin Chemistry, 2008. https://doi.org/10.1002/9780470758090.

[10] P.A. Wright, Extractive metallurgy of tin, Elsevier Scientific Publishing Company, 1966.

[11] B. Gaillard-Allemand, R. Podor, M. Vilasi, C. Rapin, A. Matre, P. Steinmetz, Experimental study of the SnO_2-ZrO_2 phase diagram, J. Eur. Ceram. Soc. 22 (2002) 2297–2303. https://doi.org/10.1016/S0955-2219(02)00034-1.

[12] C.L. Hoenig, A.W. Searcy, Knudsen and Langmuir Evaporation Studies of Stannic Oxide, J. Am. Ceram. Soc. 49 (1966) 128–134. https://doi.org/10.1111/j.1151-2916.1966.tb15390.x.

[13] M. Yamawaki, K. Yamaguchi, M. Yasumoto, Thermochemical study of vaporization of ceramic breeding materials by Knudsen effusion mass spectrometry, J. Nucl. Mater. (1991) 804–807. https://doi.org/10.1016/0022-3115(91)90210-X.

[14] E.N. Bunting, Phase equilibria in the system SiO_2-ZnO, J. Res. Natl. Bur. Standars. 13 (1930) 131–136. https://doi.org/10.1111/j.1151-

2916.1965.tb14731.x.

[15] R.A. Reyes, D.R. Gaskell, The thermodynamic activity of ZnO in silicate melts, Metall. Trans. B. 14 (1983) 725–731. https://doi.org/10.1007/BF02653959.

[16] R. Hansson, B. Zhao, P.C. Hayes, E. Jak, A reinvestigation of phase equilibria in the system Al_2O_3-SiO_2-ZnO, Metall. Mater. Trans. B Process Metall. Mater. Process. Sci. 36 (2005) 187–193. https://doi.org/10.1007/s11663-005-0019-y.

[17] L. Weber, E. Grauer-Carstensen, The solidification behaviour of melts in the system Zn_2SiO_4-Mg_2SiO_4, J. Mater. Sci. 12 (1977) 1988–1993. https://doi.org/10.1007/BF00561970.

[18] L. Xia, Z. Liu, P.A. Taskinen, Experimental determination of the liquidus temperatures of the binary (SiO_2-ZnO) system in equilibrium with air, J. Eur. Ceram. Soc. (2015) 1–6. https://doi.org/10.1016/j.jeurceramsoc.2015.07.007.

[19] S. Mihaiu, I. Atkinson, O. Mocioiu, A. Toader, E. Tenea, M. Zaharescu, Phase formation mechanism in the ZnO-SnO_2 binary system, Rev. Roum. Chim. 56 (2011) 465–472.

[20] S. Mihaiu, A. Toader, I. Atkinson, O.C. Mocioiu, C. Hornoiu, V.S. Teodorescu, M. Zaharescu, Advanced ceramics in the SnO_2-ZnO binary system, Ceram. Int. 41 (2015) 4936–4945. https://doi.org/10.1016/j.ceramint.2014.12.056.

[21] T. Yin, Coupled Thermodynamic Modeling and Experimental Study of SnO_2-SnO-CaO-SiO_2 System, (2017).

[22] I. Barin, Thermochemical data of pure substances, VCH, Weinheim, Germany, 1989.

[23] R.G. Berman, T.H. Brown, Heat capacity of minerals in the system Na_2O-K2O-CaO-MgO-FeO-Fe_2O_3-Al_2O_3-SiO_2-TiO_2-H_2O-CO_2: representation, estimation, and high temperature extrapolation, Contrib. to Mineral. Petrol. 89 (1985) 168–183. https://doi.org/10.1007/BF00379451.

[24] H. Prophet, D.R. Stull, JANAF thermochemical tables, U.S. Department of Commerce, Washington, 1985.

[25] O. Cecile, G. Patrick, Method for Producing Marked Glass Panels, WO2017FR53198 20171122, 2018.

[26] H. Spandau, E.J. Kohleymer, Das System Zinn-Sauerstoff, Zietschrift Fur Met. 40 (1949) 374–396.

[27] R.H. Insley, V.J. Barczak, Phase Equilibria in the System Al_2O_3-SnO_2, J. Am. Ceram. Soc. 45 (1962) 144.

[28] O. Ruff, Arbeiten im Gebiet hoher Temperaturen I. Über das Schmelzen und Verdampfen unserer feuerbeständigsten Oxyde im elektrischen Vakuumofen, Zeitschrift Für Anorg. Chemie. 82 (1913) 373–400. https://doi.org/10.1002/zaac.19140870113.

[29] J.C. Platteeuw, G. Meyer, The System Tin Oxygen, Dept. Gen. Inorg.

Chem. Techn. Univ. Delft. (1955) 1066–1073.

[30] X. Xu, P.C. Hayes, E. Jak, Experimental study of phase equilibria in the “SnO2”-CaO-SiO2 system in air, Int. J. Mater. Res. 102 (2011) 1208–1215. https://doi.org/10.1007/s11669-013-0241-2.

[31] K.T. Jacob, J.C. Chan, Electrochemical Determination of the Stability of Mono- and Dicalcium Stannates, J. Electrochem. Soc. 121 (1974) 534–537.

[32] H. Kopp, Investigations of the Specific Heat of Solid Bodies, Phil. Trans. R. Soc. Lond. 155 (1865) 71–202.

[33] S. Raghavan, Gibbs free energy of formation of magnesium stannate from EMF measurement, Thermochim. Acta. 122 (1987) 389–393. https://doi.org/10.1016/0040-6031(90)80520-9.

[34] A. Navrotsky, R.B. Kasper, Spinel Disproportionation at High Pressure: Calorimetric Determination of Enthalpy of Formation of Mg_2SnO_4 and Co_2SnO_4 and some Implications for Silicates, Earth Planet. Sci. Lett. 31 (1976) 247–254.

[35] K.T. Jacob, V.-N. J., Gibbs’ Free Energy of Formation of Magnesium Stannate, J. Solid State Chem. 22 (1977) 291–295. https://doi.org/10.1016/0040-6031(87)87056-9.

[36] J.A. Cerri, E.R. Leite, D. Gouvea, E. Longo, Effect of Cobalt(II) Oxide and Manganese (IV) Oxide on Sintering of Tin(IV) Oxide, J. Am. Ceram. Soc. 79 (1996) 799–804.

[37] A. Mâtre, D. Beyssen, R. Podor, Effect of ZrO_2 additions on sintering of SnO_2-based ceramics, J. Eur. Ceram. Soc. 24 (2004) 3111–3118. https://doi.org/10.1016/j.jeurceramsoc.2003.11.009.

[38] P.A. Connor, J.T.S. Irvine, Novel tin oxide spinel-based anodes for Li-ion batteries, J. Power Sources. 97–98 (2001) 223–225. https://doi.org/10.1016/S0378-7753(01)00545-6.

[39] M. Inagaki, A. Nakanishi, Y. Takeda, S. Naka, Effect of atmosphere on the formation of spinel solid solutions in Mn_2SnO_4-Mn_3O_4 system, J. Solid State Chem. 20 (1977) 323–326. https://doi.org/10.1016/0022-4596(77)90169-4.

[40] D.-J. Kim, J.-W. Jang, H.-L. Lee, Effect of Tetravalent Dopants on Raman Spectra of Tetragonal Zirconia, J. Am. Ceram. Soc. 80 (1997) 1453–1461. https://doi.org/10.1111/j.1151-2916.1997.tb03003.x.

[41] S.R. Dhage, V. Samuel, R. Pasricha, V. Ravi, Studies on SnO_2-ZrO_2 solid solution, Ceram. Int. 32 (2006) 939–941. https://doi.org/10.1016/j.ceramint.2005.06.012.

Abstract

The development of an accurate thermodynamic database to calculate the thermodynamic properties and phase equilibria in complex systems plays an important role in the development of many ceramic and metallurgical processes. Thermodynamic database is developed by the comprehensive critical evaluation and optimization of all the thermodynamic property and phase diagram data.

As part of a large thermodynamic database development for glassmaking and metallurgical applications, the entire ZnO-SnO_2-SiO_2 system was critically evaluated and optimized. Due to the lack of phase diagram experiment data in the ZnO-SnO_2, SnO_2-SiO_2, and the ternary ZnO-SnO_2-SiO_2 system, the phase equilibria in the binary and ternary systems were determined using the classical quenching experiments and differential thermal analysis (DTA) followed by X-ray diffraction (XRD) analysis and electron probe micro-analysis (EPMA). Sealed platinum capsules were employed for preventing the evaporation of ZnO and SnO_2 in the experiments. In the course of the optimization, the melting temperature of SnO_2 was re-evaluated. The phase diagrams of ZnO-SnO_2, SnO_2-SiO_2, and ZnO-SnO_2-SiO_2 systems were constructed for the first time. By using the construct thermodynamic database containing the Gibbs energy functions of all phases in the ternary system,

phase equilibria and the thermodynamic properties within the ternary system could be accurately calculated. All the thermodynamic calculations and optimization in the present study were carried out using the FactSage^{TM} thermochemical software.

Keywords: ZnO-SnO_2-SiO_2, ZnO_2-SnO_2, SnO_2-SiO_2, ZnO-SiO_2, Zn_2SnO_4, Phase Diagram, Thermodynamics, CALPHAD